



**High resolution monitoring, real time visualization
and reliable modeling of highly controlled,
intermediate and up-scalable size pilot injection
tests of underground storage of CO₂**

Contract #309067

Deliverable Number **D4.6**
Title **Modeling and interpretation of the results of the injection experiments (Part2)**

Work-Package **4**

Lead Participant **UU**
Contributors **Farzad Basirat, Zhibing Yang, Saba Joodaki, Auli Niemi (UU)**
Lurdes Martínez-Landa, Jesús Carrera (CSIC)

Date: **31.5.2018**
Dissemination level **PU**

Executive summary

This Deliverable presents the second part of model interpretations of Heletz, Israel residual trapping experiments. The actual experiments and the experimental results are described in TRUST Deliverables 2.3-2.4. In TRUST Deliverable 4.3 both the Residual Trapping Experiment I (RTE I) carried out in September 2016 and the Residual Trapping Experiment II (RTE II) carried out in August to November 2017 are modelled with 'full-physics' TOUGH2 reservoir simulations by matching the entire test sequences and obtaining best estimates for sites in-situ residual trapping. In the present Deliverable, two additional model analyses for Residual Trapping Experiment I are presented, to provide further support/confirmation to previous results. Two in-depth analyses are presented concerning specific details of Heletz Residual Trapping Experiment I (RTE I).

The first part (Chapter 1) presents a coupled wellbore-reservoir model for the period of CO₂ and CO₂/water self-release during the creation of the residually trapped zone. The observed behavior can be well matched by CO₂ exsolution in the well and reduced relative permeabilities in the formation, due to this exsolution. The model provides valuable supporting information concerning the overall behavior of the test and will later be incorporated with the overall reservoir model of RTE I (Deliverable 4.3).

The second part (Chapter 2) presents an in-depth analysis of the details of the hydraulic response of all the hydraulic tests carried out in the Heletz injection well, as part of the site characterization program and as part of RTE I. The results show that while the response of the two tests with no CO₂ in the system show a similar behaviour, the response from the test with residual CO₂ in the system is different. The storage coefficient in the well is greater, delaying the response, but the skin permeability has lower values. This behaviour can be explained by a small amount of residual CO₂ around the well, which is consistent with the other model analyses.

Altogether, the modeling carried out in Deliverables 4.3 and 4.6 will provide a good understanding of the system performance during CO₂ injection and the resulting residual trapping. The analysis work and summarizing the results will continue beyond the time of final reporting for TRUST and the resulting peer-reviewed publications will be uploaded to the TRUST web-site.

Keywords	Heletz CO ₂ injection, residual trapping experiments, coupled wellbore-reservoir flow, hydraulic well-test analysis
----------	--

Table of Contents

1. Characterization of CO₂ self-release during Heletz Residual Trapping Experiment I (RTE I) using a coupled wellbore-reservoir simulator	3
1.1 Introduction	3
1.2 CO ₂ withdrawal by opening the well (Self-release).....	3
1.3 Methodology.....	4
1.3.1 Analysis of CO ₂ volume fraction.....	4
1.3.2 Numerical simulator T2Well/ECO2N	4
1.3.3 Conceptual model and model development	5
1.3.4 CO ₂ mobility scenarios.....	7
1.4 Results	8
1.4.1 Analysis of CO ₂ volume fraction.....	8
1.4.2 Results of the numerical modeling	9
1.5 Discussion and conclusions.....	14
2. In-depth interpretation of hydraulic tests with and without CO₂ in the formation	14
2.1 Introduction	14
2.2 Methodology.....	17
2.2.1 Step 1: Detrending and data treatment (drawdowns and pumping rates)	18
2.2.2 Step 2: Transforming recovery heads into drawdowns	20
2.2.3 Step 3: Smooth log-derivatives.....	25
2.3 Site description.....	28
2.4 Results	28
2.4.1 Analytical interpretation	28
2.5 Numerical model.....	40
2.5.1 E1 test.....	40
2.5.2 E2 test.....	42
2.5.3 E3 test.....	43
2.6 Discussion.....	46
3. Conclusions	47
4. References:.....	48

1. Characterization of CO₂ self-release during Heletz Residual Trapping Experiment I (RTE I) using a coupled wellbore-reservoir simulator

1.1 Introduction

Heletz CO₂ injection experiments (RTE I and RTE II) have been carried out by creating a residually trapped zone of CO₂ in the formation and characterizing the system by different means before and after creating this zone. The difference in the outcome of these characterization tests provides information of the residually trapped zone (e.g. Niemi et al. 2016, Rasmusson *et al.* 2014). In the first experiment, the Residual Trapping Experiment I, done on September 2016, the residually trapped zone was created by injection of CO₂, then withdrawing CO₂ thereby leaving the residual zone behind. The CO₂ withdrawal stage consisted of two parts. First, the well was opened to the atmosphere and CO₂ was released spontaneously, first only CO₂ and then CO₂ with water. In the second stage, fluids were actively pumped with air-lift until the formation was deemed to be at residual stage.

In this section of the report, we especially focus to the CO₂ self-release part, which as such causes uncertainty in CO₂ mass balance when the processes in the reservoir are modelled. Understanding and rigorously modelling this complex process also furthers the overall understanding of processes in the reservoir and wellbore during the injection-withdrawal experiment.

For the modeling, we use a coupled well-reservoir simulator T2Well-ECO2N (Pan & Oldenburg 2014, Pan *et al.* 2011b) that has been specifically developed for geological storage of CO₂. In the following text, we will shortly describe the self-release behavior observed in September 2016. We then proceed to the analytical analysis of CO₂ volume fraction, model development and numerical simulations with well-reservoir simulator T2Well-ECO2N. This is followed by an analysis of the results, discussion and conclusions.

1.2 CO₂ withdrawal by opening the well (Self-release)

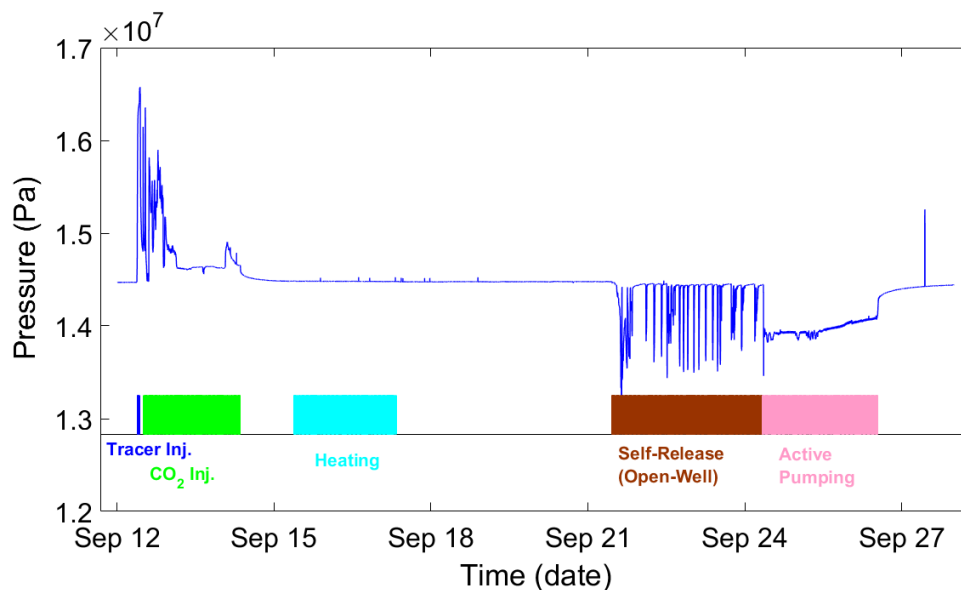


Figure 1. Heletz test sequence (September 2016) and measured pressure at depth of 1617.35 m.

During the self-release period, the pressure measurements in the bottom of wellbore chamber show cycling pressure fluctuation during the period of self-release (red interval in Figure 1). This pressure behavior seen in Heletz is very similar to natural CO₂ geysers (Watson *et al.* 2014, Lu *et al.* 2006, Lu *et al.* 2005). So, the mechanisms defining geyser eruption described by Lu *et al.* (Lu *et al.* 2006) can be applied to explain the pressure fluctuation during the CO₂ self-release. Each cycle (pressure dropping) is considered to begin when the water level has recovered from an earlier low level to reach the top of the well and the pressure has its maximum value and temperature at its lowest. No degassing will occur until CO₂ becomes supersaturated in the water. Pressure reduction because of the upward flow of CO₂-rich fluids will initiate exsolution. The flash depth (FD) marks the depth where CO₂ in aqueous phase initially starts to exsolve. Above the FD, the exsolved CO₂ bubbles migrate upwards due to lower density of CO₂(g) than liquid water. Then the upwardly migrating CO₂ bubbles will merge and create larger bubbles and slug flow. The overflow or eruption continues by reducing the hydrostatic pressure, and consequently the FD deepens (from the surface) within the well. Finally the CO₂ exsolution depth will also reach its maximum that is, the well chamber. Due to excessive degassing, eruptions will cease once the CO₂(aq) concentration has reached a critical minimum, waiting for completion of another recharge from the reservoir. This combined process of CO₂-driven eruption shows self-enhancing and self-limiting behavior and results in the periodic eruption scenarios observed (Watson *et al.* 2014).

1.3 Methodology

1.3.1 Analysis of CO₂ volume fraction

In the Heletz test, the pressure and temperature variations monitored are given for two depths at the well bottom. Sensor PT-76 is located at the depth of 1632.91 m and PT-78 is located at the depth of 1617.35 m. Both sensors are located inside the well chamber. The pressure difference can be used to determine the mixture (CO₂ and water) density and volume fraction of CO₂ in the well chamber between the two sensors by using a simple analytical approach suggested by Lu *et al.* (Lu *et al.* 2005). In this method, the pressure differences between the two points let us to determine the mean density of the fluid mixture and its local average void fraction by means of following equations:

$$\rho_m = \frac{P_{78} - P_{76}}{gh} \quad (1)$$

$$\alpha = 1 - \frac{\rho_m}{\rho_L} \quad (2)$$

where in these equations α is the volume fraction, ρ_L is the brine density, g is the gravitational acceleration and h is the distance between the two pressure sensors. In this calculation, the only uncertain parameter is the brine density that depends on salinity, temperature and pressure conditions in reservoirs can vary between 1007 kg/m³ and 1020 kg/m³. In this calculation, the mean value for the liquid density ($\rho_L = 1013.5 \text{ kg/m}^3$) is used.

1.3.2 Numerical simulator T2Well/ECO2N

T2Well is an extended version of TOUGH2 numerical simulator for modeling non-isothermal, multi-phase, and multicomponent fluid and energy flow in coupled well-reservoir systems (Pan & Oldenburg 2014,

PanWebb & Oldenburg 2011, Pan et al. 2011b). The multiphase flow in the wellbore is simulated by solving one dimensional momentum equation. The velocity of two-phases is described by DFM (Drift Flux Model) (Shi *et al.* 2005). By applying the DFM, the two-phase momentum equations are lumped into a single momentum equation for fluid mixture (Pan & Oldenburg 2014). A summary of the mathematical formulations that are implemented in T2Well can be found in the T2Well/ECO2N manual (Pan & Oldenburg 2014). Like TOUGH2, T2Well needs to be used with different equation-of-state (EOS) modules to describe different fluid mixtures. In this work, we used module ECO2N that includes equations-of-state for two-phase flow (gas and liquid), three mass components (water, salt, and CO₂) over the ranges of pressure and temperature of interest in this study. In ECO2N, the term 'gas phase' refers to the CO₂-rich phase and the term 'liquid phase' refers to the water-rich phase. It should be noted that CO₂ in 'gas phase' could be formally gaseous, liquid, or, supercritical CO₂, depending on the pressure and temperature conditions. However, by this terminology CO₂ in the liquid phase is CO₂ dissolved in water or brine.

1.3.3 Conceptual model and model development

Opening the valve for CO₂ withdrawal (self-release) results in pressure gradient in the wellbore and upward flow of CO₂ and water through the well in to the atmosphere. The pressure monitoring measurements at two points in the wellbore as well as flow rates data at the top of the well are going to be compared with the numerical simulations results. To model the self-release test, a simple conceptual model representing the site was constructed based on geological and petrophysical data. The model and the parameter values (Table 1) are based on the site characterization data available (Niemi et al. 2016) as well as results and calibration from the previous modelling of the injection experiments that were carried out (Deliverable 4.3).

Table 1. Properties and parameter values used for the modeling

Parameter	Value	Unit
Well Length	1448	m
Well Diameter	0.073	m
Thermal conductivity	3.30	W/m C°
Reservoir length	1.0	km
Boundary conditions at wellhead	P = 0.1035 T = 35	MPa C°
Roughness parameter	0.046 × 10 ⁻³	m
Absolute permeability	H1 = 650 H2 = 450	mD mD
Porosity	H1 = H2 = 0.25	
Salinity	0.05	NaCl mass
Initial conditions	Gas saturation, pressure and temperature at the end of rest time (at 21-sep-2016 11:15) from numerical simulation.	
Outer boundary condition	No-flow	

The Heletz Experiment conceptual model (Figure 2) consisted of two high-permeable layers (noted here as H1 and H2), 2 and 9 m thick, respectively, separated by a 3 m thick low-permeable layer (L1) and overlaid by an additional low-permeable layer (L2). The bottom depth is assumed –1641 m, with the top

of the uppermost low-permeable layer located at -194 m. An impermeable layer with a constant temperature of 65 °C was assumed to underlay the wellbore and storage formation. The thermal heat transmission from the wellbore to the surrounding rocks formations is treated numerically. The thermal properties of surrounding rocks are simply assumed homogeneous for all rocks. We developed a radially symmetric grid for T2Well to simulate the configuration in the well and its coupling to the surrounding reservoirs, cap rock, and upper formations (Figure 2). For the initial and boundary condition, we used the simulation results of gas saturations and pressure after the injection and resting period before the opening well (Figure 3).

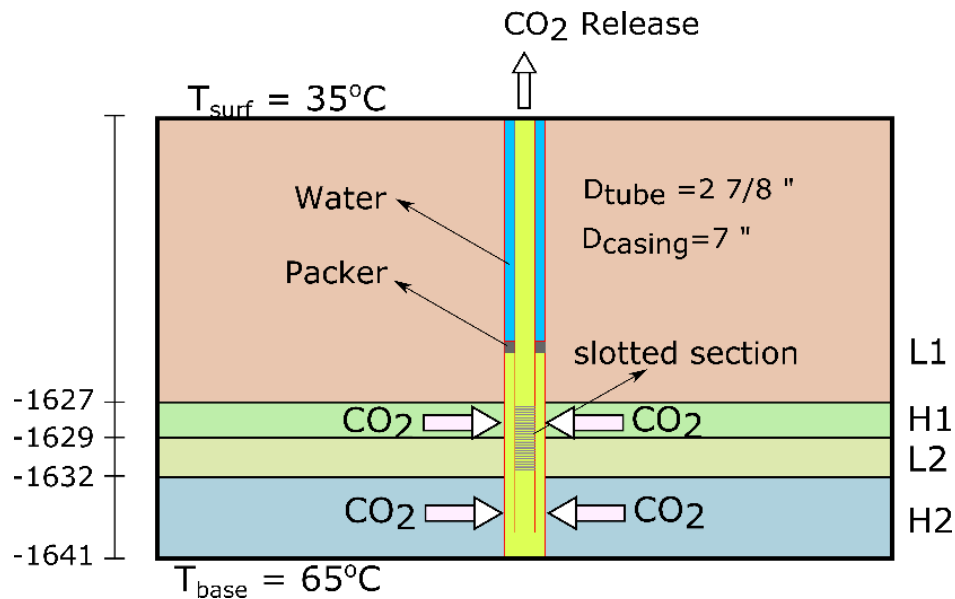


Figure 2. Conceptual model (not to scale) showing Heletz test reservoirs (H1 and H2), low permeable layers (L1 and L2), and wellbore for CO₂ self-release period.

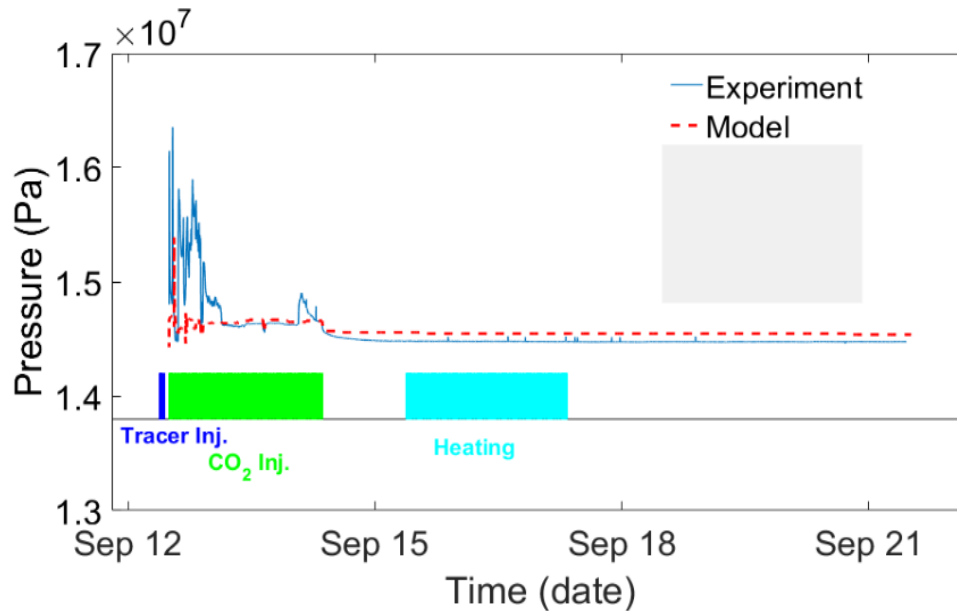


Figure 3. Measured pressure and numerically modelled pressure (at depth of 1617.35 m) along with test sequences.

1.3.4 CO₂ mobility scenarios

The pressure behavior suggest that gas mobility in reservoirs is less than the measurement from core experiments (Hingerl et al., 2014, Niemi et al, 2016). This hypothesis is based on both on experience from CO₂ natural geysers and numerical simulations. The numerical simulations by Pan et al, (Pan et al. 2011a) suggest that the gas saturation in the reservoir to be only slightly above the residual gas saturation for the geyser behavior to happen. The geysers behavior happens, when the gas phase inflow into the wellbore, as controlled by reservoir transmissivity, is not high enough. In addition, natural CO₂ geysers show that the CO₂ in reservoirs is in residual form and the mobile CO₂ phase is result of exsolution from CO₂ saturated brine in the system.

In addition, the core experiments by Zuo et al, (Zuo et al. 2013, Zuo et al. 2012) show a strong reduction of reservoir relative permeability in the presence of exsolved CO₂. This is due to pressure reduction, creating a large amount of separated CO₂ bubbles that reduce the relative permeability. This phenomenon has been established both at the pore and core scales (Zuo et al. 2017, Zuo et al. 2013, Zuo et al. 2012, Xu et al. 2017).

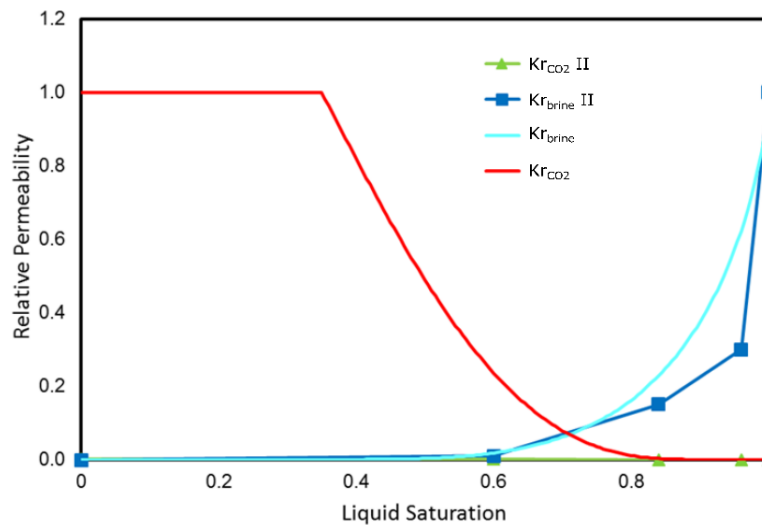


Figure 4. Relative permeability of CO₂ and brine used in numerical simulation of CO₂ self-release. The lines without marks are based on core data from Heletz (Hingerl *et al.* 2016, Niemi *et al.* 2016) and marked lines show the reduced relative permeabilities based on Zuo *et al.* (2012).

Subsequently, two different sets of relative permeability curves were used (Figure 4). In scenario (I) the relative permeabilities measured on Heletz cores (Hingerl *et al.* 2016) were used while in scenario (II) a reduced relative permeability for both CO₂ (green with triangle marker) and brine (blue with square marker) were used as defined by Zuo *et al.* (2012) to represent the reduced values due to exsolution.

1.4 Results

1.4.1 Analysis of CO₂ volume fraction

Figure 5 shows the measured pressure differences between the two sensors. The pressure difference has fluctuating behavior. When the difference is lower more CO₂ phase is present between the two sensors while higher values correspond to more water and less CO₂. Figure 6 shows the calculated volume fraction of CO₂ or gas saturation between the two sensors of PT76 and PT78 based on this pressure data. The gas saturation is approximately between 0.01 and 0.10.

CO₂ (g) evolves in well chamber between sensors when pressure is reduced. There are two possible sources for this gas, namely CO₂ exsolving from water and injected gaseous CO₂. From this analysis, the source of CO₂ filling the column between two sensors cannot be determined. It can, however, be seen that the CO₂ flow in wellbore is taking place faster than the accumulation of CO₂ into chamber.

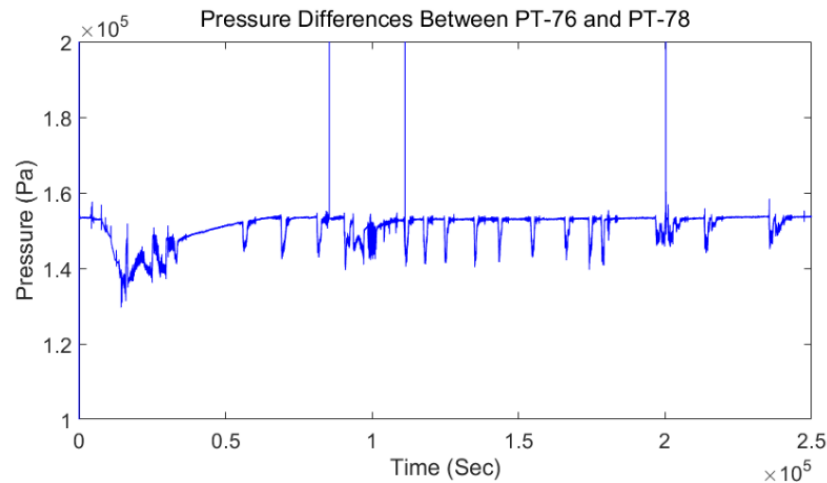


Figure 5. Pressure difference between sensors PT76 and PT78 during the self-release period.

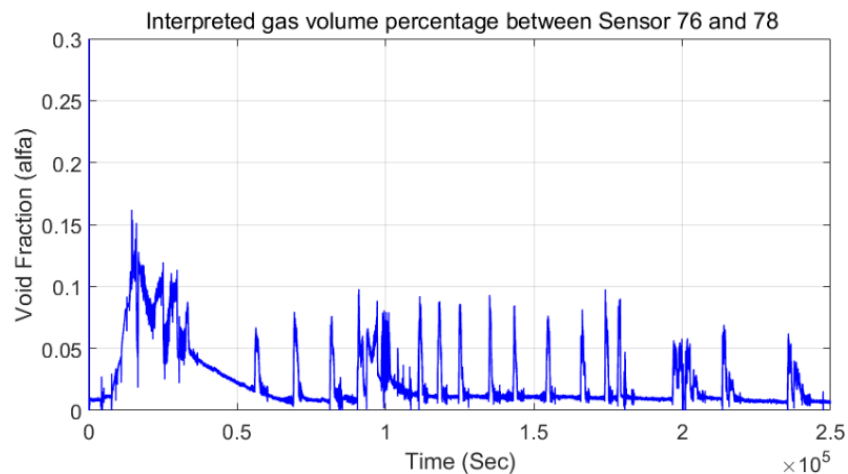


Figure 6. Interpreted CO₂ volume fraction between sensors PT76 and PT78 during the self-release period.

1.4.2 Results of the numerical modeling

1.4.2.1 Scenario 1: relative permeability as determined from the cores

Figure 7 shows the simulated and measured pressures at 1617.35 m depth in the well. It can be seen, that the results show no good agreement. The pressure values from numerical simulation show continuous behavior while the measured data shows the geysering one. The simulated pressure drops at about 1000 seconds and after that, increases in three steps. The sudden drop in the pressure is caused

by the breakthrough of the gas flow, when the bottom and the middle of the wellbore are filled by 40, respective 70 percent, with gas (Figure 8). The presence of gas reduces the density and consequently the pressure. The pressure values then increase with gas inflow reduction at the bottom of wellbore, as shown in Figure 9. The gas phase in the wellbore moves faster in the upper half of the wellbore than lower half, due to density reduction and slug flow (Pan et al. 2011a). This process is known as the self-acceleration effect. The rapid sweep of water through the wellbore occurs around 2000 sec (Figure 10). This peak in gas flow rate (Figure 9) reflects a burst effect of the high pressure gas flow.

This result suggest that the gas mobility in reservoir has to be lower than the relative permeabilities determined from the core experiment would correspond to. Figure 9 and Figure 10 show both gas and liquid inflow to the bottom of well being reduced by passing time. This can be explained by pressure depletion in the reservoir.

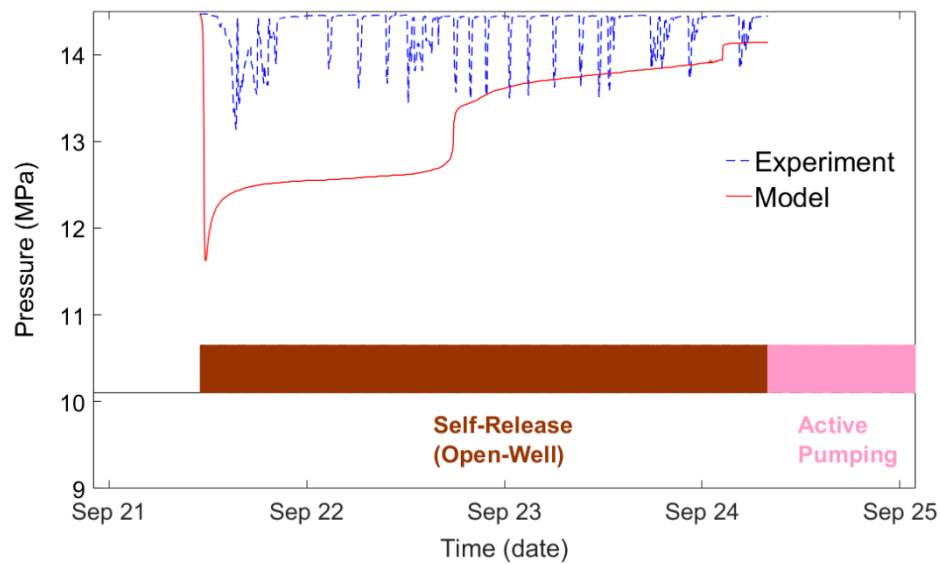


Figure 7. Measured pressure and numerically modelled pressure (at depth of 1617.35 m) along with test sequences for the first scenario with original relative permeability.

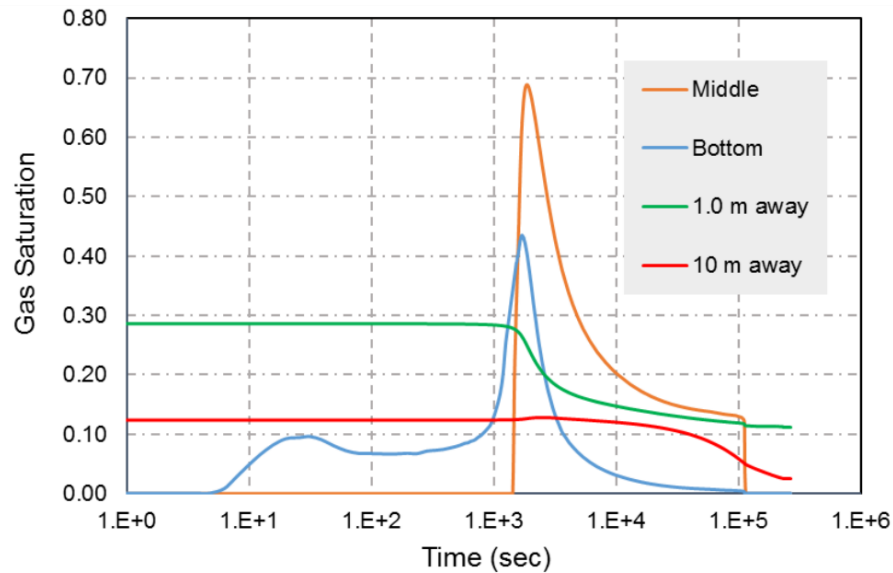


Figure 8. Simulated gas saturation at two levels in the well (bottom and middle), and two locations in the upper reservoir for the base scenario with measured core relative permeability.

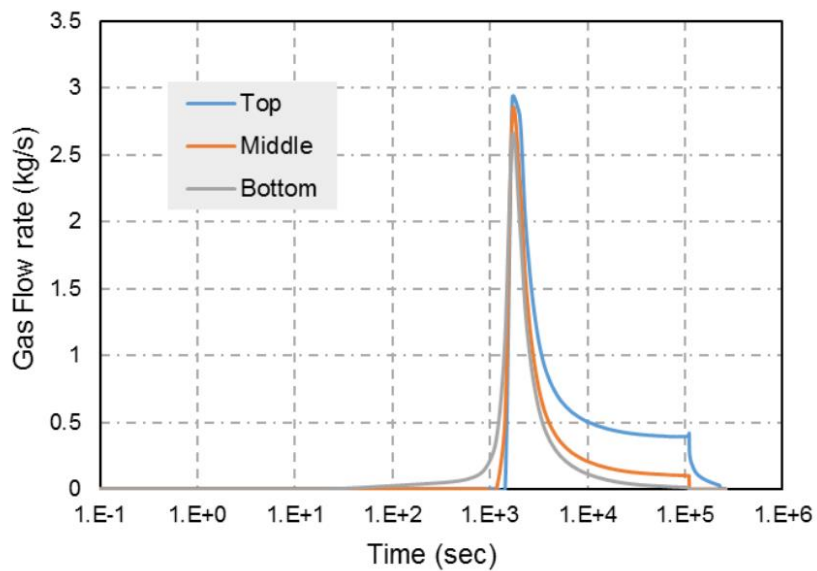


Figure 9. Simulated gas flow rate at three levels in the well (bottom, middle, and top) for the base scenario with measured core relative permeability.

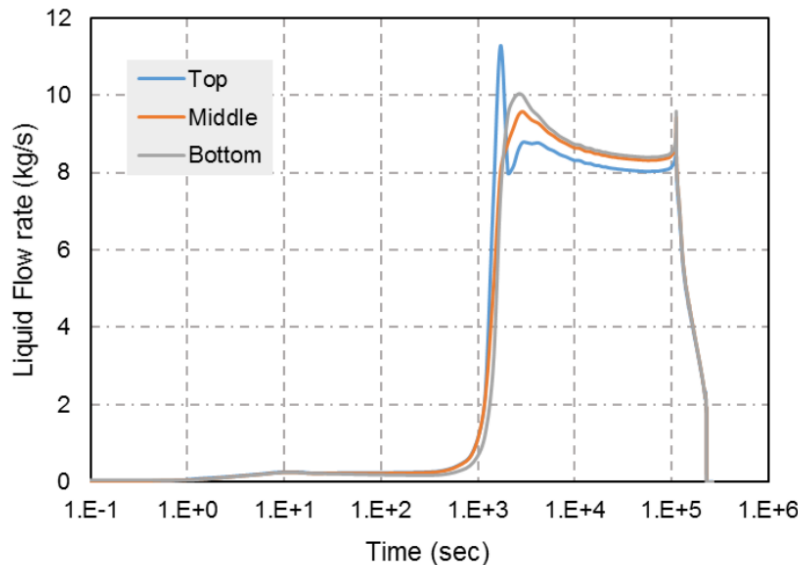


Figure 10. Simulated liquid flow rate at three levels in the well (bottom, middle, and top) for the base scenario with measured core relative permeability.

1.4.2.2 Scenario 2: relative permeability of exsolution

In the second scenario the mobility of the CO₂ gas phase in the reservoir was reduced by reducing the gas relative permeability by about 10⁻⁴ - 10⁻⁵, as suggested by Zuo et al, 2012 (Zuo et al. 2012). The relative permeability of water is also reduced slightly at high water saturations. Using this assumption describes a condition where the only source of gas inflow into the well is CO₂ exsolution from water. All other conditions are kept the same as in the previous scenario.

Figure 11 shows the simulated pressure for these updated relative permeabilities along with the measured data. The comparison shows a significantly improved agreement, with similar shape in the pressure fluctuation. This indicates that the assumption of no or very small gas mobility appears to capture the measured behavior.

There is a difference in the magnitudes of the pressure drops, the simulated ones being somewhat larger than those in the data. This can be explained by the fact that the wellbore model is developed for CO₂ and brine in the well and the part that is unsaturated consisting of air is not taken into account. Ignoring this unsaturated part of the wellbore can influence the simulated pressure drop. At Heletz the depth of the unsaturated zone is about 194 m. Therefore, this can retrieve some part of pressure drop at the bottom in comparison to the situation modeled.

Overall, even the density of the fluctuations is very similar. It should be pointed out that the first part of the oscillations in the data that are not captured with the model, coincides with the period when only CO₂ was observed to be released, not water.

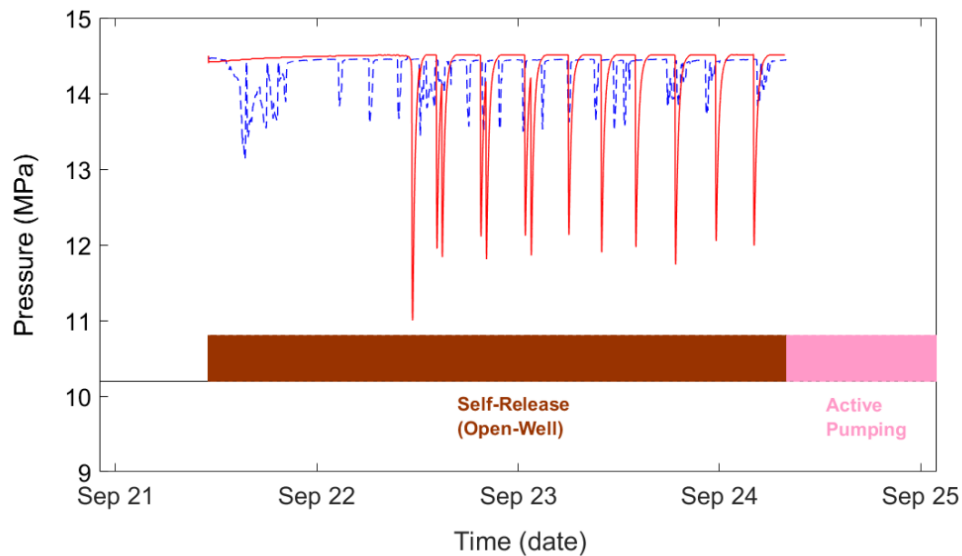


Figure 11. Measured pressure and numerically modelled pressure (at depth of 1617.35 m) along with test sequences for the second scenario with modified relative permeability.

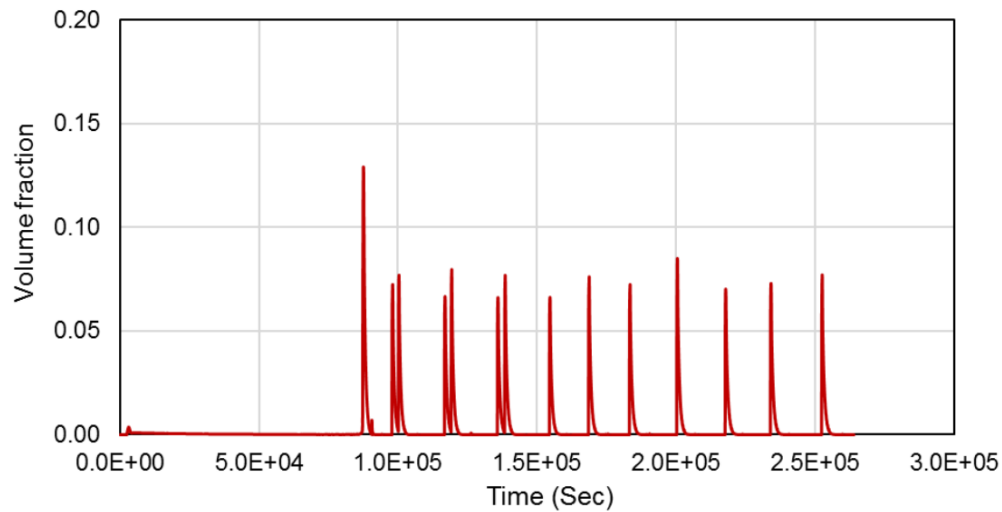


Figure 12. The simulated volume fraction of CO₂ between the two sensors.

Figure 12 shows the simulated volume fractions of CO₂ between the two sensors at the bottom of the wellbore. Comparison of the volume fractions calculated analytically based on the pressure difference in the well (Figure 6) and the numerically simulated values in Figure 12 shows a good agreement for the

part of the experiment where both water and gas were released (in the early part there was gas release only). Both show values of the order of 7% or so, the data showing somewhat more irregular and towards the end decreasing tendency that the simulated values. Overall, the agreement can be considered very good for this type of model.

1.5 Discussion and conclusions

In Heletz Residual Trapping Experiment I (RTE I), part of the creation of the residually trapped zone consisted of first opening the well to the atmosphere and allowing the CO₂ to escape without any pumping. In the beginning, only pulses of CO₂ were released, then for most of the period, fluctuating pulses of CO₂ and water. In the down-hole pressure and temperature sensors this period shows as oscillating, periodic pressure and temperature response. Similar oscillating pressure behavior has been seen in natural CO₂ geysers such as Crystal and Tenmile geysers in Utah (Watson et al. 2014). The mechanism driving natural CO₂ geysers is due to CO₂-degassing or, in other terms, CO₂ exsolution process in the wellbore.

With the knowledge of such exsolution process, a conceptual model was built for the borehole-reservoir system that firstly used the measured relative permeability functions (scenario 1), the reduced relative permeability functions, to take into account the effect of exsolution as suggested by Zuo and co-workers (scenario 2). The results show that the latter model is able to capture the observed behavior very well, a very encouraging result.

Previous core- and pore-scale experiments by Zuo et al, (Zuo et al. 2017, Zuo et al. 2013, Zuo et al. 2012) have shown that pressure decrease can indeed considerably reduce the CO₂ mobility in the porous media. Later studies could address in more detail the underlying mechanisms for similar reduction at Heletz. For this, also the Uranine tracer recovery data (See Deliverable 2.3-2.4) could provide additional information. During the experiment, Uranine tracer was injected immediately before the CO₂ injection. Recovery of the tracer during the self-release period can give additional indication of mobile versus residual CO₂ in the reservoir. Further modeling is needed to address this issue. In the future, further sensitivity analyses will also be carried out to further examine the effect of well and reservoir properties on pressure fluctuations during the self-release, as well as to integrate the results of the present model to the more detailed reservoir model presented in Deliverable 4.3.

2. In-depth interpretation of hydraulic tests with and without CO₂ in the formation

2.1 Introduction

This chapter contains a detailed interpretation of all the hydraulic tests at CO₂ injection well H18A of Heletz, carried out firstly as part of the site characterization, then as part of the first residual trapping experiment. One pumping test was performed on December 2013 as part of site characterization (see Niemi et al., 2016). Two additional tests were performed in September, 2016, one before the injection of CO₂ and creation of the residually trapped zone, and one after, as part of the Residual Trapping Experiment I (RTE I). The objective of these two latter tests was to characterize residual CO₂, which should display as a reduction in permeability and an increase in storativity (see Martinez-Landa et al., 2013).



The impact of the reduction in permeability (Figure 13 A&B) is significant, but it is hard to derive residual CO₂ saturation from the reduction in transmissivity. Residual CO₂ is much better characterized by the increase in storativity around the well, but its effect is more subtle (a slight retardation in the time drawdowns reach radial flow conditions), which in practice will be hard to distinguish from wellbore storage. Therefore, exquisite test performance and interpretation are required. To facilitate interpretation, the idea of the Heletz experiments was to perform two tests, one before and one after CO₂ push-pull (so as to leave some CO₂ trapped in the aquifer).

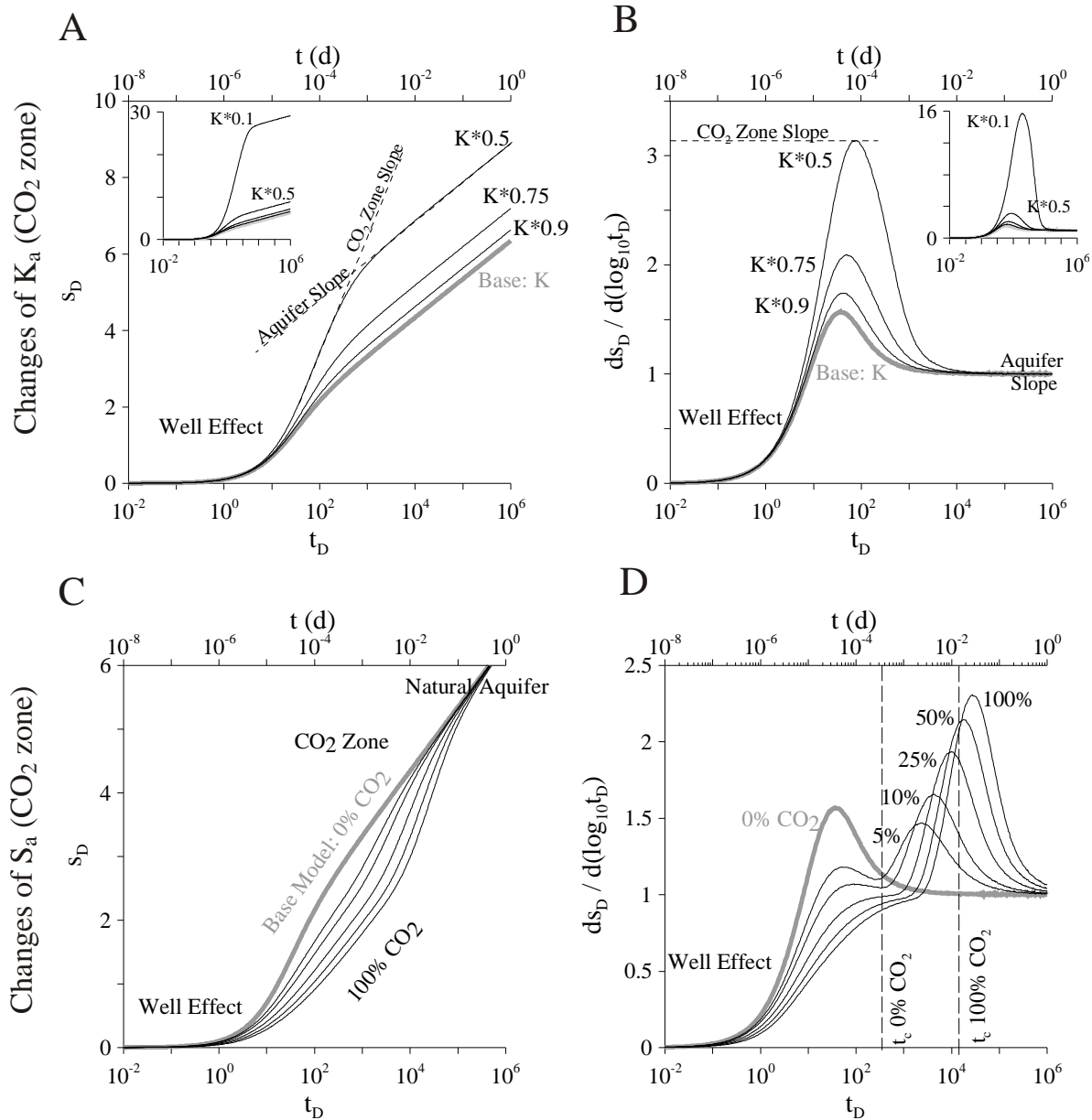


Figure 13. Effect of the reduction in permeability (top row) and increase in storage (bottom row) caused by trapped CO₂ around a well. The left graphs display drawdowns whereas the right graphs display log-derivatives (Martinez-Landa et al., 2013).

Traditional interpretation of pumping tests consists of the following steps.

Step 0: Remove trends so as to be able to isolate drawdowns that can be attributed to the tests from environmental fluctuations (e.g., seasonal changes in recharge, tidal effects, uncontrolled nearby pumping, stage changes in close rivers, etc.), which may dominate small head responses (e.g., far away

observation points or late time recovery) and must be filtered out prior to interpretation (see, e.g., Halford et al. 2012).

Step 1: Diagnostics. Plot drawdowns and their logarithmic derivative to gain insight into the type of aquifer and the appropriate model (Bourdet et al., 1983, 1989)

Step 2: Interpret the test either graphically (from the log-log and semi-log plots) or numerically (using a flow model).

This methodology is hard to apply in practice because the diagnostic plots are hard to obtain. Difficulties arise because: (1) detrending may be problematic when heads fluctuate for unknown reasons; (2) diagnostic plots rely on constant pumping rate which is often hard to keep (electrical failures, well development, pump characteristics, well going dry, etc) ; and (3) log-derivatives tend to be extremely noisy, which hinders their interpretation.

The Heletz experiments did not suffer from the first difficulty because the site is quiet. Pumping in the aquifer is limited and far away, so that heads tend to be constant. However, the pumping tests badly from noise in the data and, especially, from fluctuating flow rate. Since the natural heads are low (some 300m deep) pumping had to be done by air-lift, which fluctuates and is hard to measure because water coming out at the well-head is mixed with a high proportion of air.

To overcome these two difficulties, we propose a new interpretation methodology that relies on:

1. Interpret recovery (when pumping rate is zero and, therefore, well known) rather than pumping phase data. The traditional "Theis recovery method" is robust, but yields little information about the aquifer model, as required by Figure 13. Therefore, we propose using Agarwal (1980) and a modified approach to obtain a drawdown curve similar to the one that would have been obtained during pumping. Both methods have been analysed by Trabucchi et al (2018), as part of TRUST.
2. Acknowledge variations in pumping rate during the pumping phase. To this end, we have developed equations that allow correcting the recovery time depending on the variability of pumping rates (Trabucchi et al 2018).
3. Compute smooth log-derivatives from noisy drawdown data. To this end, we have derived a variational regularization approach (Ramos et al, 2017).

We explain the details of the methodology in 2 and then apply the methodology to the Heletz tests in 4.

2.2 Methodology

The proposed methodology consists of four steps, which we propose as an alternative approach to perform and interpret hydraulic tests, beyond the experiments at Heletz. The basic assumption is that the test has been performed by:

1. Pumping a well with a controlled pumping rate. It is desirable that the pumping rate be constant, at least during the second half of the pumping period, but it is not essential. Since interpretation is going to be based on the recovery, it is important to record accurately (to the second) the time at which pumping stopped.
2. Measuring the pumping rate over time
3. Measuring head or relative pressures over time since well before the beginning of pumping until well after the end. Ideally, heads should be monitored for a period comparable to pumping duration before the start, and for some 10 times the pumping duration after.

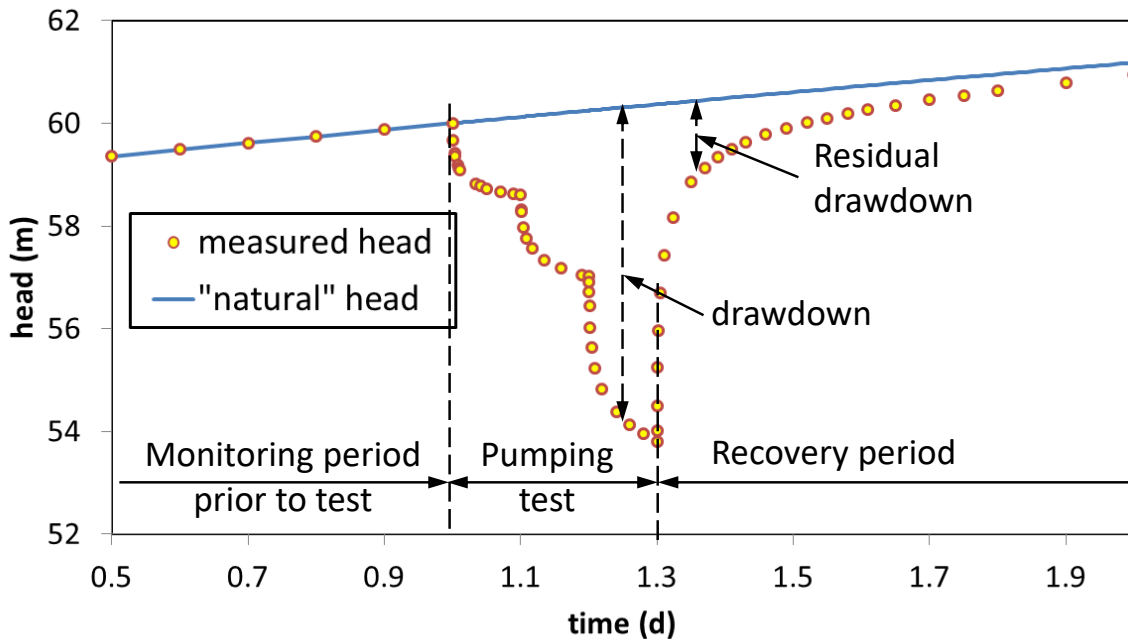


Figure 14. Drawdowns are the difference between the (ideal) natural heads and measured heads during a pumping test. Drawdowns during recovery are termed “residual drawdowns”.

As mentioned in the introduction, the proposed approach is specifically applicable to cases in which the pumping rate is variable and hard to control, so that interpretation concentrates on recovery data. The methodology consists of four steps, of which our contributions concentrate in steps 2 and 3. While the procedure refers to pumping test (recovery data) interpretation, it yields some implications specific recommendations for the performance of the test. These are discussed at the end.

2.2.1 Step 1: Detrending and data treatment (drawdowns and pumping rates)

This step refers to (1) the derivation of drawdowns (including residual drawdowns, see Figure 14) from head measurements and (2) the definition of pumping rates.

2.2.1.1 Drawdown

Drawdown is defined as the difference between natural heads, h_N , which would have been observed if pumping had not occurred and the actually observed heads, h_P (see Figure 14).

$$s(x, t) = h_N(x, t) - h_P(x, t) \quad (3)$$

The reason for this definition is discussed below. The important thing is that h_N obeys the flow equation

$$S_s \frac{\partial h_N}{\partial t} = \nabla(\mathbf{K}\nabla h_N) + r_N \quad \text{in } \Omega \quad (4)$$

Where S_s is specific storage, \mathbf{K} is hydraulic conductivity, and r_N is (natural) recharge. This equation is subject to (natural) initial and boundary conditions:

$$h_N(x, t = 0) = h_{N0}(x) \quad \text{in } \Omega \quad (5)$$

$$K\nabla h_N \mathbf{n} = \alpha(h_N - H_N) + Q_N \quad \text{in } \Omega \quad (6)$$

where Ω is the flow domain and Γ its boundary, α is a leakage factor and Q_N is the natural boundary flux. These (natural) heads are not observed because of pumping. Assuming that the external head, H_N , and boundary flux, Q_N , are not affected by pumping, the heads that actually occurred (affected by pumping) are governed by:

$$S_s \frac{\partial h_p}{\partial t} = \nabla(K\nabla h_p) + r_N + \delta(\mathbf{x}_p)Q_p \quad \text{in } \Omega \quad (7)$$

$$h_p(\mathbf{x}, t = 0) = h_{N0}(x) \quad \text{in } \Omega \quad (8)$$

$$K\nabla h_p \mathbf{n} = \alpha(h_p - H_N) + Q_N \quad \text{in } \Gamma \quad (9)$$

Where \mathbf{x}_p is the location of the pumping well and Q_p the pumping rate.

The implication of Eqs. 7-9 is that modeling h_p implies including not only the pumping test, but also all natural factors. This is, in general, complex and would make test interpretation difficult. This is why, instead of working with heads, it is better to work drawdowns (Eq. 3). The equations governing drawdowns are obtained by subtracting Eqs. 7–9 from Eqs. 4–6, which leads to:

$$S_s \frac{\partial s}{\partial t} = \nabla(\mathbf{K}\nabla s) - \delta(x_p)Q_p \quad \text{in } \Omega \quad (10)$$

$$s(x, t = 0) = 0 \quad \text{in } \Omega \quad (11)$$

$$\mathbf{K} \cdot \nabla s \cdot \mathbf{n} = \alpha s \quad \text{in } \Gamma \quad (12)$$

Notice that these equations are formally identical to those controlling h_N or h_p , but adopting homogeneous boundary and initial conditions (zero heads and fluxes) and neglecting natural recharge. The drawdown equations 10–12 only include the pumping that causes drawdowns.

Two important consequences of Eq. 3 are:

(1) The drawdown concept does not require initial steady conditions or absence or recharge. These conditions are usually required for pumping test interpretation.

(2) Drawdown is not initial head minus observed head, as usually defined, but “natural” head (i.e., the head that would have been observed if pumping had not occurred) minus the observed head.

Obviously, the problem is that h_N is not known. Furthermore, there is no established technique to estimate it. In general, heads fluctuate due to a broad range of natural reasons.

- Recharge; which typically fluctuate seasonally, but which may also change suddenly (e.g. rainfall during the test).
- Unknown pumping at neighboring wells (if it is known, it can be included as part of the test).
- Tidal fluctuations at the boundary (e.g., sea tides) or within the domain (e.g., Earth tides)
- Barometric fluctuation, ET cycles and a long etc.

The point is that is difficult to account for all of them. While many of them may be considered small (and are often neglected), they can still late time recovery. A number of options are available to handle them:

1. Filter out known causes of fluctuations (see Halford, xxx) for details.
2. Use neural networks (Coppola et al., 2003, 2005) to estimate h_N , by calibrating (training) the neural network using heads prior to the test and, possibly, long after as output, and records of heads at neighboring wells unaffected by the test, as input.
3. Approximate $h_N(t)$ at observation positions using a simple function of time (typically polynomial), whose parameters are calibrated using heads prior to the test and, possibly, long after.

The summary of this discussion is that heads, at the pumping and observation wells, need to be monitored for long before and after the test in order to be able to filter natural trends.

2.2.1.2 Flow rates

2.2.2 Step 2: Transforming recovery heads into drawdowns

2.2.2.1 Agarwal and proposed methods

Recovery data (i.e., residual drawdowns measured after pumping has stopped, (recall Figure 15) are much less noisy than pumping data because pumping rate variability does not affect the aquifer response directly but only indirectly. The traditional method for recovery data interpretation is Theis Recovery Method (Theis, 1935), which consists of plotting residual drawdown (ideally, $s_R(t) = s(t) - s(t - t_p)$) versus $t_R = t/(t - t_p)$ and deriving transmissivity from the resulting slope in semi-log scale. The method is quite robust in estimating effective transmissivity values over a region that grows with the duration of pumping (Willmann et al. 2007; Copty et al. 2011), but lacks the worth of information about the aquifer behavior contained in constant rate pump test data (this will be revised in the next section). Numerous methods have been introduced to overcome this limitation, which suggests that recovery data contain information similar to that of the pumping phase of the test. Most of these methods are straight-line-methods based on Cooper & Jacob (1946) (CJ in the following) approximation that allow evaluating hydraulic parameters, but do not yield any information about the conceptual model. Yet, Agarwal (1980) introduced a method, based on CJ’s approximation, to reproduce the response of a pumping test using recovery test data. In other words, his method permits plotting recovery data as if they resulted from constant rate pumping, facilitating not only the estimation of hydraulic parameters, but also conceptual model assessment. Here, we describe this method and an alternative method.

Agarwal initially developed his method for recovery test interpretation with the implicit assumption of an ideally large, homogeneous and confined aquifer, subject to a constant pumping rate from a fully penetrating well for a sufficiently long time. Under these conditions, flow towards the well is radial, and the CJ equation yields a good approximation for late time drawdowns, i.e., $s(t) = (Q/4\pi T) \ln(2.25Tt/r^2S)$,

where Q is pumping rate and r is distance to the center of the pumping well or effective radius of the well when computing drawdowns at the pumping well itself. Based on the superposition principle, this author defined what we now call Agarwal drawdown as (Figure 15):

$$s_A(t) = s(t_p) - s_R(t) = s(t_p) - (s(t) - s(t - t_p)) \quad t > t_p \quad (13)$$

where t is the time elapsed since the beginning of pumping, t_p is the time at the end of pumping, and $s_R(t)$ is the (Theis) residual drawdown. The latter "will be the same as if discharge of the well had continued but a recharge well with the same flow had been introduced at the same point at the instant discharge stopped" (Theis 1935).

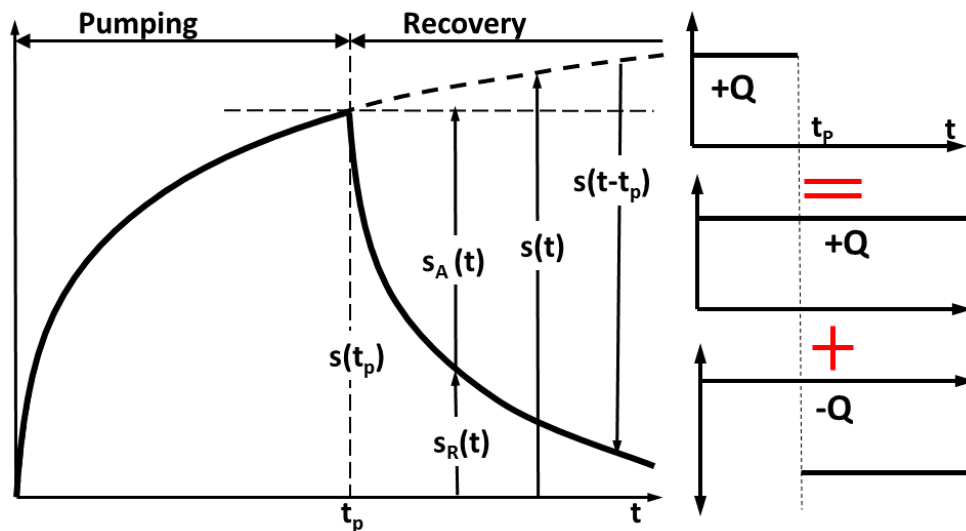


Figure 15. Pumping and recovery test. The left graph displays the residual drawdown, s_R , used in Theis recovery method and Agarwal's drawdown, s_A . Both can be computed by superposition (right) of a continuous pumping (+ Q) and an injection (- Q) that start at the time t_p when pumping stopped in reality.

That is, superposition implies that $s_R(t) = s(t) - s(t - t_p)$. Agarwal then used the CJ's approximation to the three drawdowns appearing in equation (1), which yields:

$$s_A(t) = \frac{Q}{4\pi T} \left[\ln\left(\frac{2.25Tt_p}{r^2S}\right) - \ln\left(\frac{2.25Tt}{r^2S}\right) + \ln\left(\frac{2.25T(t-t_p)}{r^2S}\right) \right] = \frac{Q}{4\pi T} \ln\left(\frac{2.25T}{r^2S} t_A\right) \quad (14)$$

The resulting equation has exactly the same form as that of CJ for a pumping test, but using t_A , implicitly defined as $t_A = t_p(t - t_p)/t$, instead of t . Therefore, Agarwal proposed, without further justification, treating s_A versus t_A as the drawdown curve caused by pumping Q . This is quite surprising because the CJ's approximation does not hold for small recovery times $(t - t_p)$, and, yet, the method works fine.

Four nice features of this approximation are worth pointing. First, t_A is comparable to $(t - t_p)$ when t_p and t are comparable (i.e., when t_p is large). Second, when t tends to infinity, t_A tends to t_p , i.e., Agarwal's method will not yield a (pumping) drawdown curve longer than the pumping period. Third, s_A can be obtained directly from measured variables (drawdown at the end of pumping and residual drawdown). Fourth, as we shall see, the method works quite well. All of them explain the success of the method in the oil industry, where application is immediate, as the test simply consists of monitoring the pressure build-up after well shut-in.

Trabucchi et al. (2018) show that a problem with Agarwal method is that it requires a relatively long pumping time and suggest using CJ's approximation, or any other that the modeler deems appropriate to transform the recovery test drawdown information into that of a pumping test:

$$s_M(t - t_p) = s_{ap}(t) - s_R(t) \quad , t > t_p \quad (15)$$

where $s_{ap}(t)$ is an approximation of $s(t)$ that depends on the modeller's assumption about the behavior of the system. The two most immediate options are (1) $s_{ap}(t) = s(t_p) + m \cdot \ln(t/t_p)$, if the modeler assumes that flow is radial (dimension $n = 2$) and that a constant slope has been reached; or (2) $s_{ap}(t) = s(t_p) + (2m/(2 - n)) \left((t/t_p)^{1-n/2} - 1 \right)$, if the modeler assumes a power-law behavior of the log-derivative (i.e., that flow occurs with a dimension n other than 2). In either case, m is the log-derivative at the end of the pumping phase, or the slope of the drawdown data, divided by 2.3, if they are plotted versus $\log_{10} t$ (traditional CJ semi-log plot).

This new approximation (Eq. 15) differs from that of Agarwal (Eq. 13) as the delay in the aquifer response after pumping shut down is taken into consideration. In fact, instead of a constant value $s(t_p)$, an extrapolated function $s_{ap}(t)$ has been considered to evaluate the pumping test drawdown that would have occurred at $t > t_p$ if a longer pumping test had been carried out. As the defined function is a straight line with slope m , the new approximation $s_{ap}(t)$ tends to CJ's one if quasi steady radial regime has been reached. Otherwise, in transient regime, a straight line with a lower slope will be generated. The latter condition is easy to meet in observation wells where the characteristic time is greater compared to that of the pumping well. Consequently, the aquifer response shows a delay (drawdown may increase for some time after pumping shut in) that can be seen as if the pumping time period would last longer than that in the pumping well. As Agarwal's method was originally developed to analyze data recorded in the pumping well itself (as usually done in the oil and gas industry), the aquifer system behavior for transient time is not taken into account and insufficient pumping time periods lead to negative Agarwal's drawdown.

Applying the proposed method, it is important to underline that 1) we use recovery time $(t - t_p)$ to plot residual drawdown, that means plot data on the same time scale of that of producing time; 2) the evaluation of s_M can be easily performed using the last pumping time data and recovery data series; 3) as we shall see, the method works quite well, allowing to obtain early-time data curves from recovery data even when the dimensionless duration of pumping is short; but (4) late time values of $s_M(t)$ are virtually identical to $s_{ap}(t)$ because $s_R(t)$ tends to zero (recall Figure 15). Because of this last remark, $s_M(t)$ should not be used for recovery times longer than the pumping test duration.

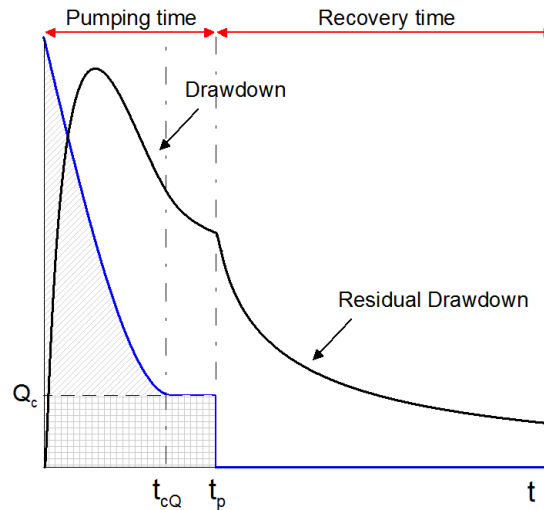


Figure 16. Response to a pumping test carried out applying a variable pumping rate. The pumping rate decrease with the time, becoming constant for a while after pumping shut down (Trabucchi et al., 2018).

2.2.2.2 Variable pumping rate

We generalize here Agarwal, Theis and other methods to acknowledge time-dependent pumping rate during the interpretation of recovery data. Time variability of pumping rate has been addressed by numerous authors, including Agarwal (1980). The goal has been typically to interpret pumping test data and the method consists of using either superposition (Birsoy & Summers 1980) or deconvolution (Schroeter et al. 2002). Given the difficulties of the latter, and the specificities of recovery test analysis, we adopt an approach similar to that of Birsoy & Summers (1980), but taking advantage of the fact that the last portion of the pumping phase is often performed at a constant rate. Therefore, we assume that the pumping rate fluctuates only up to time t_{cQ} (Figure 16). Trabucchi et al. (2018) show that drawdown after t_{cQ} can be calculated as if pumping rate had been constant, and equal to Q_c , substituting time, t , by $tE_I(t)$, where E_I is defined as:

$$E_I(t) = \exp \left[\int_0^{t_{cQ}} \frac{1}{Q_c} \frac{dQ'}{d\tau} \ln \left(\frac{t-\tau}{t-t_{cQ}} \right) d\tau \right] \quad (16)$$

We illustrate the use of Equation (16) by application to a step drawdown test with $Q(t) = Q_i$, $t_i \leq t < t_{i+1}$, $i = 1, N$, where N is the number of steps, and $t_N = t_{cQ}$ (pumping rate is Q_c during the last step), then $dQ'/d\tau = \sum_{i=1}^N (Q_i - Q_{i-1}) \delta(t_i - \tau)$, with $Q_0 = Q_N = Q_c$ (Figure 17). With these definitions,

$$E_I(t) = \prod_{i=1}^{N-1} \left(\frac{t-t_i}{t-t_{cQ}} \right)^{\Delta Q_i / Q_c} \quad (17)$$

where $\Delta Q_i = Q_i - Q_{i-1}$. This equation is similar to those of Birsoy & Summers (1980) and Agarwal (1980), except that they add each step independently. In the case of Birsoy and Summers (1980), their choice made sense because they were seeking an approximation of drawdown during pumping, but it is somewhat less accurate if Q' is indeed small and zero after t_{cQ} .

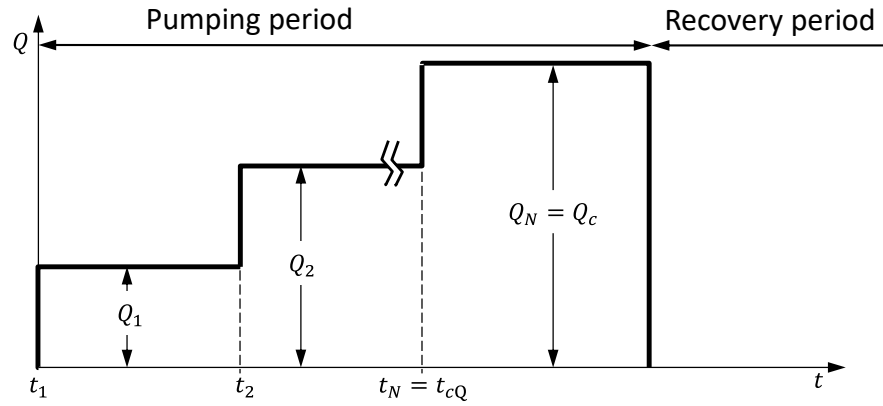


Figure 17. Nomenclature for variable pumping rate.

Mishra et al. (2013) argued that step approximations may not be appropriate for smoothly varying flow rates and proposed a Laplace transform solution for time-wise linear flow rate. Equation 9 can also be easily integrated in this case. Assume that the pumping rate varies linearly between point measurements, $Q(t_i) = Q_i$, $i = 1, N$, with possible jumps at t_1 [$\Delta Q_1 = Q_1 - Q_c$] and $t_N = t_{cQ}$ [$\Delta Q_{N+1} = Q_c - Q_N$], when E_I becomes (again easy but tedious integration)

$$E_I(t) = \left(\frac{t-t_1}{t-t_{cQ}}\right)^{\Delta Q_1/Q_c} \left(\frac{t-t_N}{t-t_{cQ}}\right)^{\Delta Q_{N+1}/Q_c} \prod_{i=2}^N \left(\frac{t-t_{i-1}}{e(t-t_{cQ})}\right)^{\Delta Q_i/Q_c} \left(\frac{t-t_{i-1}}{t-t_i}\right)^{m_i(t-t_i)/Q_c} \quad (18)$$

where $e = 2.718$ is the Euler's number. The "equivalent time", $tE_I(t)$, can be used for all approximations of drawdowns caused by pumping (but not by recovery). Therefore, Agarwal drawdown for variable pumping rate becomes

$$s_{Ac}(t) = s(t_p) - s_R(t) = \frac{Q_c}{4\pi T} \cdot \ln \left[\frac{2.25T t_p(t-t_p)E_I(t_p)}{r^2 S tE_I(t)} \right] \quad (19)$$

Which suggests a modified Agarwal time:

$$t_{Am} = \frac{t_p(t-t_p)E_I(t_p)}{tE_I(t)} \quad (20)$$

With the new corrected time t_{Am} , it becomes feasible to interpret recovery test data, as the mark left by the past flow history over the recovery signal has been taken into consideration. Obviously, this equivalent time should be used also for Theis recovery method [$t_R = tE_I(t)/(t - t_p)$] or for the proposed alternative.

Trabucchi et al. (2018) analyze the impact of neglecting pumping rate variations on both Agarwal method and note that it may be severe. Therefore, they concluded that proper interpretation of recovery data requires accounting for pumping rate variability. This conclusion is almost trivial (after all, a pumping test consists of measuring the head response to pumping), but it is often taken for granted and pumping rate variability goes unaccounted for.

2.2.3 Step 3: Smooth log-derivatives

2.2.3.1 Log-derivatives: concept and usefulness

An ideal pumping test consists of extracting a constant flow rate from a well and observing the resulting drawdowns at the same well and, possibly, one or several observation wells. Hydraulic parameters are obtained by fitting observed drawdowns with a model. Since Theis (1935), a large number of models have been developed to represent various features of the aquifer (presence of boundaries, leakage from adjacent formations, delayed yield, etc.) or the well itself (wellbore storage, partial penetration, etc.). These models are fitted to data numerically or graphically. The former is usually necessary for complex models. Yet, visual inspection of data is needed to identify the best conceptual model. Model identification is based not only on the understanding of the aquifer, but also on the observed drawdowns themselves. Unfortunately, the abundance of models can be their nemesis because the differences between model responses may be so subtle that model selection often becomes ambiguous.

This ambiguity has been greatly reduced through the use of log-derivative plots (derivative of drawdown with respect to the logarithm of time). These were introduced by Chow (1952) and refined by Rai (1985), Yeh (1987), and especially Bourdet et al. (1983, 1989), who introduced it in the oil industry, providing an effective method to calculate log-derivatives and generalizing the approach for any type of models. These plots are called diagnostic plots when both drawdowns and log-derivatives are plotted together in log-log and semi-log scales. Their relevance stems partly from the fact that the log-derivative is the slope of the semi-log plot of drawdowns, which is inversely proportional to transmissivity in homogeneous models (Theis, 1935; Cooper and Jacob, 1946), to the effective transmissivity in stationary heterogeneous media (Meier et al., 1998) or, in general, to the transmissivity in the region of growth of the cone of depression (Butler, 1988). However, their use goes far beyond.

The log-derivative highlights small variations in the shape of drawdown curves, thus facilitating the identification of the model, which is useful if the real aquifer is well represented by one the documented models, an assumption that must be verified independently, typically on the basis of geological and geophysical information. The concept of log-derivative and diagnostic plots is illustrated in Figure 18 Renard et al. (2009) provide an excellent account of the log-derivative plots for different models, which is informative even if the aquifer is not well represented by an existing model, because the log-derivative depends on the flow geometry and permeability away from the pumping well. Some of them are shown in Figure 19 which illustrates that indeed log-derivatives help in identifying the conceptual model.

2.2.3.2 Computation of log-derivatives

The problem of log-derivatives lies on how to compute them. In principle, the problem can be formulated as that of computing an approximation of the derivative of drawdowns s , given n noisy observations $\{(x_i, s_i)\}$, $i = 1, \dots, n$, where $x_i = \ln(t_i)$. Formulated in this way, the problem is quite conventional in numerical analysis. Unfortunately, numerical differentiation is ill-posed because small errors in the data may cause large changes in the corresponding derivative. The problem is particularly severe in well hydraulics, where data tend to stabilize at late time, where measurement devices resolution is limited and where measurement intervals may be variable.

Two families of methods emerge. The first one is based on direct numerical derivation of the data. The most popular one in the oil industry is the one of Bourdet et al. (1989);

$$u_i \cong \frac{\frac{\Delta s_L \Delta x_R + \Delta s_R \Delta x_L}{\Delta x_L \Delta x_R}}{\Delta x_L + \Delta x_R} \quad (21)$$

Where $\Delta s_L = s_i - s_{i-l}$, $\Delta s_R = s_{i+r} - s_i$, $\Delta x_L = x_i - x_{i-l}$, $\Delta x_R = x_{i+r} - x_i$, and l and r are selected such that Δx_L and Δx_R are similar. The value Δx , which represents a log time cycle fraction, is typically quite small (0.01

to 0.2), depending on the data density. Note that Equation (1) is the conventional centered incremental ratio when $\Delta x_L = \Delta x_R$ and that a small increase in Δx may imply a significant increase in smoothing, while a small decrease may imply instability. To control smoothing and instability Bourdet et al. (1989) propose choosing an optimal step size. A number of alternatives have been selected to overcome the problems of numerical derivatives, such as computing the log-log derivative (Hosseinpour-Zonoozi, 2006), or using different number of points in the formulae Anderssen et al. (1984). But, the truth is that all methods yield noisy derivatives.

The method of Ramos et al (2017) can be formulated as: given noisy observations $\{(t_i, s_i), i = 1, \dots, n\}$ where $s_i = s(t_i)$, we seek an approximation of the derivative function $u = s' = \partial s / \partial \ln t$ in the interval $[t_1, t_n]$. Note that the problem is essentially identical for the computation of the log-log derivative, $(\partial \ln s / \partial \ln t)$. In essence, we need to minimize the errors in drawdowns resulting from the integration of the derivative and to penalize fluctuations in the derivative. This can be achieved by finding u , as the function that minimizes the functional

$$F(u) = F_s(u) + \lambda F_d(u) = \frac{1}{2} \int_{x_1}^{x_n} \omega(x) (Au - y)^2 dx + \frac{\lambda}{2} \int_{x_1}^{x_n} \beta(x) \left(\frac{du}{dx}\right)^2 dx \quad (22)$$

where, $F_s(u)$ measures errors in drawdowns and F_d penalizes abrupt log-derivatives, $x = \ln(t)$, $y = s - s_1$, $Au(x) = \int_{x_1}^x u(x') dx'$ is the anti-differentiation operator, λ is the regularization parameter; $\omega(x)$ allows assigning varying weights to different portions of the drawdown data, which may be useful to relax fitting when drawdowns are unreliable, and $\beta(x)$ allows the same for derivatives, which may be useful to relax smoothing at times when the derivative plot displays high curvature.

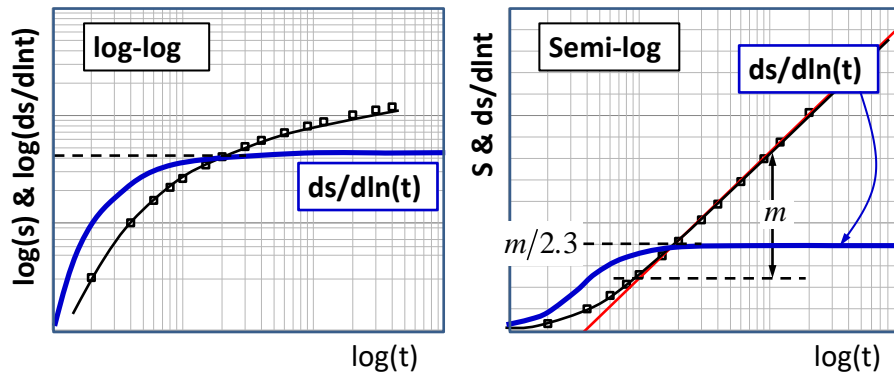


Figure 18. Diagnostic plots include drawdown and derivative graphs. Both log-log (left) and semi log (right) graphs are useful. In the pure radial flow case, the derivative tends to a constant ($m/2.3$). The 2.3 factor reflects that derivatives are taken with respect to $\ln(t)$, while the slope m is obtained graphically from the semi-log graph, where the logarithm is decimal. for variable pumping rate.

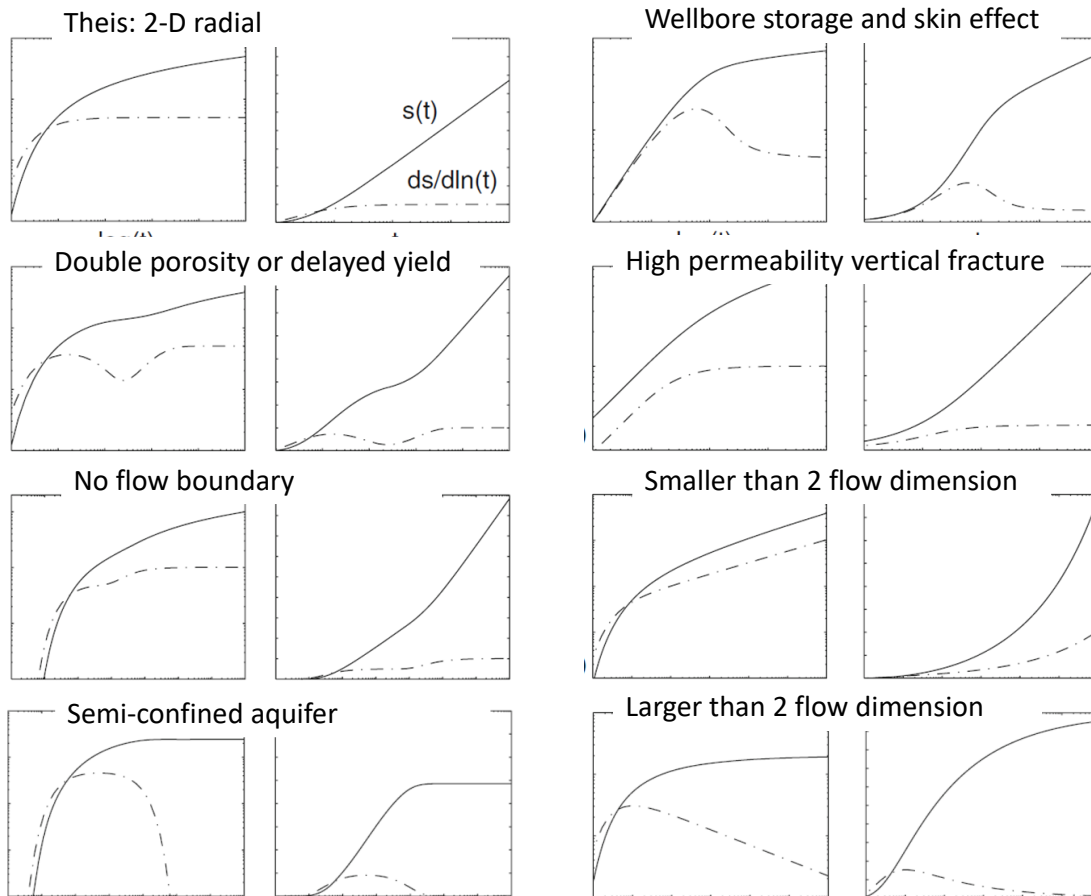


Figure 19. Diagnostic plots for a number of models (modified after Renard et al., 2009).

The last term of this functional is identical to the one representing dissipation energy in groundwater flow, in which case u would represent head and $\beta(x)$ hydraulic conductivity. Minimizing such a functional leads to the steady-state flow equation and was widely used in early formulations of the finite element method (e.g., Neuman and Witherspoon, 1970) and in upscaling the effective transmissivity in flow through heterogeneous media (Indelman and Dagan, 1993).

To minimize this functional, we make zero the variational derivative of (2) with respect to u , which leads to the differential equation:

$$\lambda \frac{\partial}{\partial x} \left(\beta \frac{\partial u}{\partial x} \right) - A^T (\omega (Au - y)) = 0 \quad (23)$$

where $A^T f(x) = \int_x^{x_n} f(x') dx'$ is the adjoint operator of A .

Solution of equation (5) requires specifying boundary conditions (B.C.). These can be of different types, depending on the information that can be deduced from the data and from the conceptual understanding of the system. If the log-derivatives are known at the ends of the observation interval, then $u(x_1) = y'(x_1)$ and $u(x_n) = y'(x_n)$, where $y'(x_1)$ and $y'(x_n)$ are assumed known (Dirichlet B.C.). These values can be

obtained from the data. However, well hydraulics understanding may provide more interesting information about the most appropriate boundary condition. For example, $y'(x_1)$ should be 0 at an observation point whose response is highly delayed with respect to the beginning of observations. A Neumann B.C. ($\partial u(x)/\partial lnt = 0$) can be assumed at late time under radial flow, when the log-derivative is constant. Cauchy B.C. ($\partial u(x)/\partial lnt = mu(x)$) may be adequate at both ends of the interval, because it represents power-law behavior, where m is the power-law exponent:

$$u = u_0 \left(\frac{t}{t_0}\right)^m \Rightarrow \frac{\partial u}{\partial lnt} = mu_0 \left(\frac{t}{t_0}\right)^m = mu \quad (24)$$

where u_0 is the log-derivative at t_0 . This B.C. may be used to represent actual power law behavior, frequent in fractured media (e.g., Gringarten et al., 1974; Beauheim et al., 1988). But it may also be used to represent the even more frequent constant derivative (i.e., $m = 0$) case, indicative of Theis like behavior. It can also be used when observations start during the interval dominated by wellbore storage, in which case $m = 1$.

We have programmed the solution of Eq. (23) with any type of boundary conditions and it is available both as a FORTRAN code and as a spreadsheet.

To estimate λ , we use the *L-curve* method (Neuman and de Marsily, 1976; Castellanos et. al., 2002). The L-curve is a parametric curve that is generated plotting in a log-log scale the smoothing criteria ($1/2 \int \beta(x)(du/dx)^2 dx$) versus the fitting criteria ($1/2 \int \omega(x)(Au - y)^2 dx$) for every value of λ . Hopefully the plotted curve will have an L-shape, which reflects the conflict between good fitting of drawdowns (e.g., . A balanced λ is chosen as the value that produces the maximum curvature of the L-curve, i.e. the corner of the L.

The interpretation has been made transformed pressure measurement in drawdowns (deducting first measurement as steady data), the flow rate used is a constant Q_c value (calculated in Step 3). Maximum information from the results is obtained representing pressure recover in two different ways. Pressure recovery (s) vs logarithm of time and derivative of pressure recovery vs logarithm of time, both in the same graphic. This graphic are drawn in simple and double logarithm scales.

2.3 Site description

The reservoir is geologically composed by three sand layers, K, W and A (Heletz sand formation), separated between them by clays. The reservoir is overlaid by a limestone layer LC-11 (Figure 20).

2.4 Results

2.4.1 Analytical interpretation

It follows the methodology applied to the test interpretation of the three tests E1, E2 and E3, as it has been explained in the methodology section:

Step 1; Detrending and data filtering (pressures and flowrates). Step 2; transforming recovery heads into drawdowns. Step 3; smoothing the data.

2.4.1.1 E1 test

The original data seem to be previously filtered, with measurements every minute. The drawdowns have a clear trend (Figure 21), the last part of recovery data showing negative values. This trend cannot be corrected because the original data start at the very beginning of the test time.

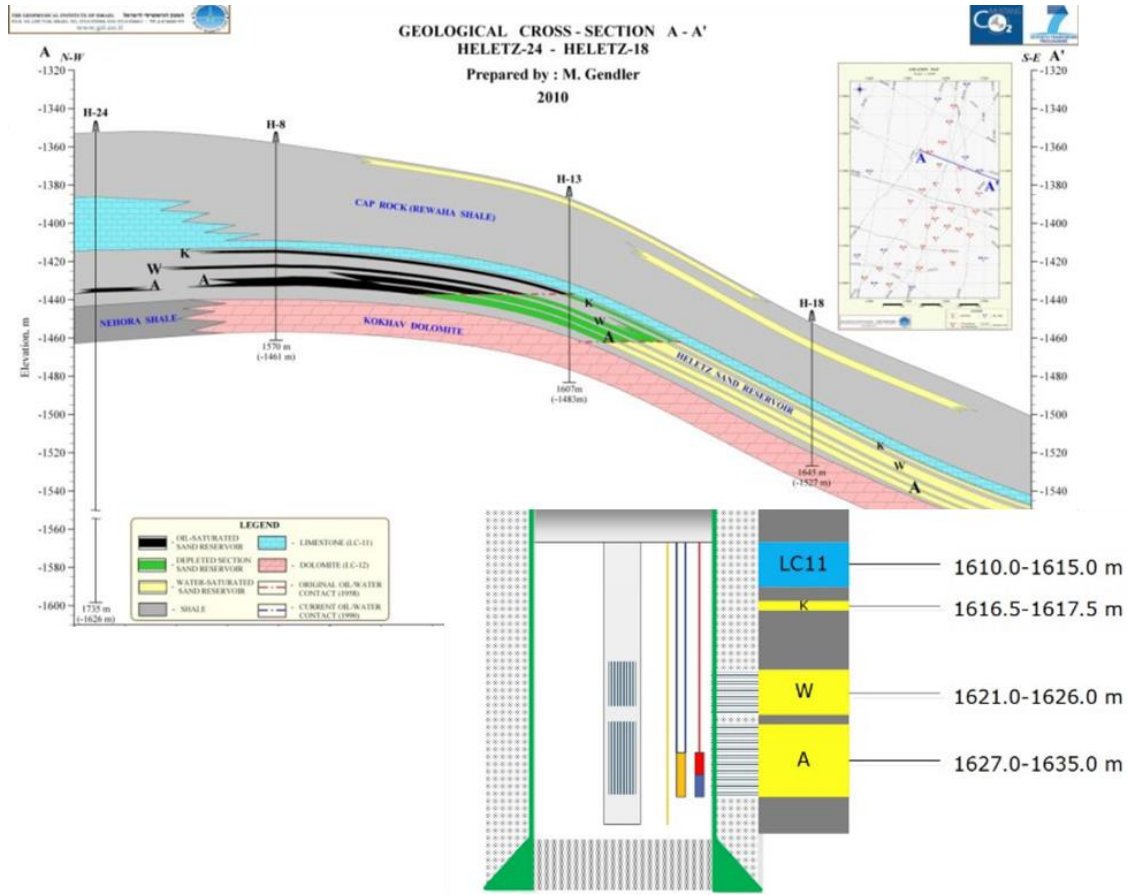


Figure 20. Geological layers at Heletz site (after Niemi et al., 2016).

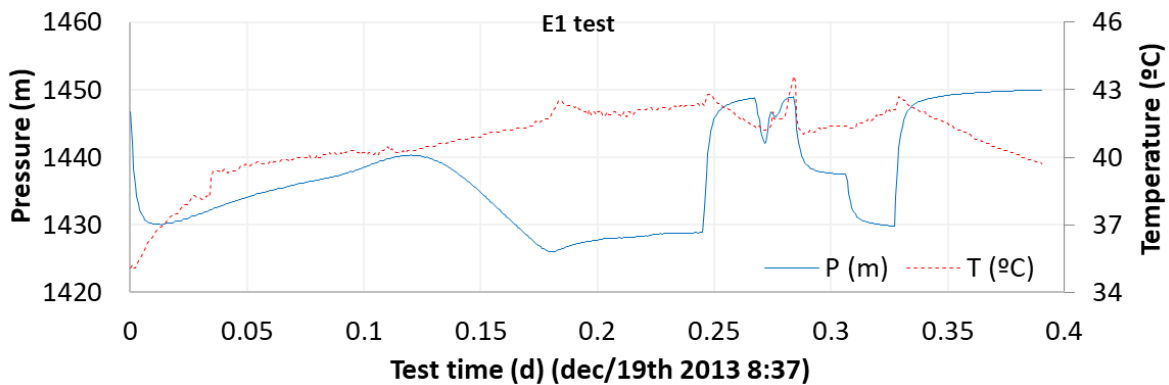


Figure 21. Original pressure (blue line) and temperature (in red) measurements.

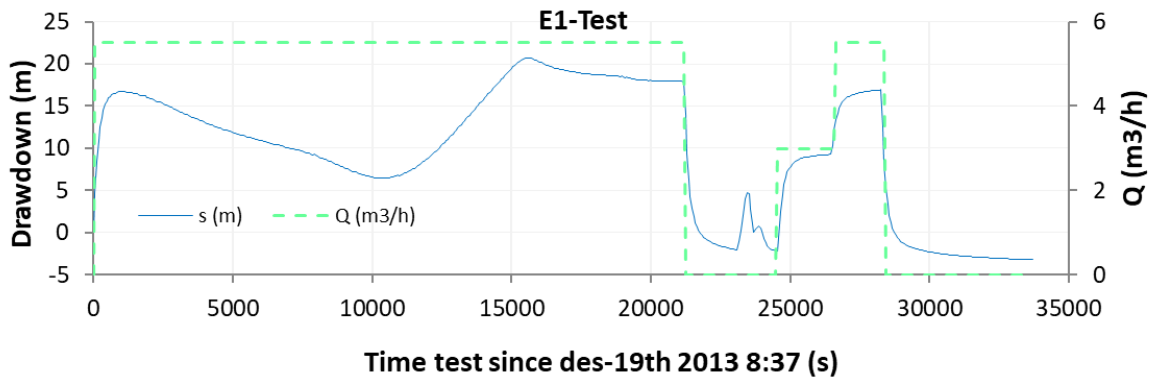


Figure 22. Calculated drawdowns from initial pressure measurement (blue line) and flow-rate measurements (in green).

The original drawdown data file has been filtered (or simplified) rudely, since the flowrate is assumed to be constant in the first two steps whilst there are increases and decreases on pressure (Figure 22).

Table 2 shows the main data from pressure responses: E1-1 is the first flowrate step prior to the first stop of the pump ($Q=0$) and E1-2 is the change in pressure between E1-1 and the definitive stop of the pump. We have analyzed this last stop as the recovery of pressure using first $Q=0$ as a flowrate step (Figure 22).

The parameters obtained from the slopes of semi-log curve are shown in Table 3. First slope is due to the skin effect, around the well walls. This value is smaller than the one of the aquifer because of the fine sediments accumulated around the borehole.

Table 2. E1 test main times from pressure measurements.

E1-1	Data	Test time [d]	Test time [s]
Start time	12/19/2013 8:37	0	0
Stop pumping time	12/19/2013 14:30	0.245	21180
Final Recovery time	12/19/2013 15:25	.283	24480
E1-2	Data	Test time [d]	Test time [s]
Start time	12/19/2013 15:25	0	0
Stop pumping time	12/19/2013 16:30	0.045	3900
Final Recovery time	12/19/2013 17:59	0.107	4240

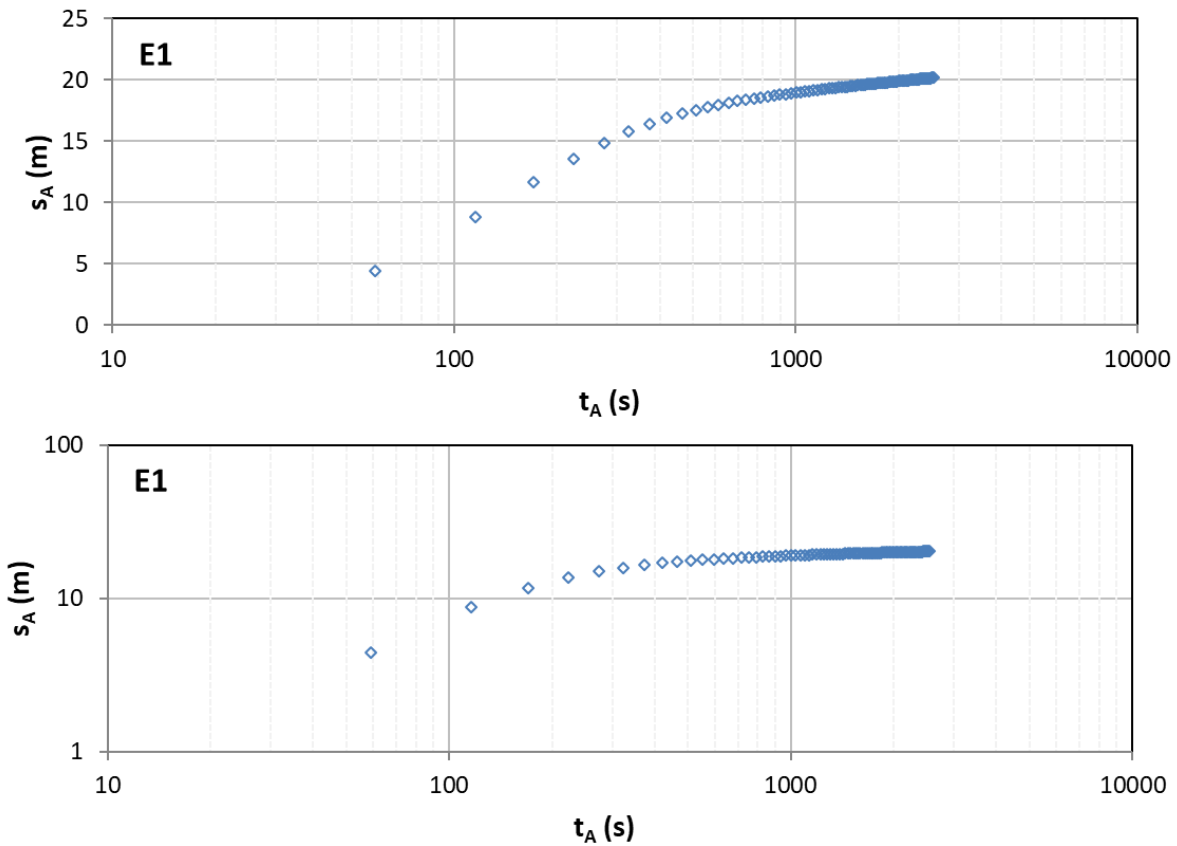


Figure 23. Transformation of pressures during recovery to drawdowns using Trabucchi et al 2018 method.

Figure 23 plots the drawdown calculated with the Trabucchi et al 2018 method.

The smoothed and filtered E1 recovery data are shown in the Figure 23. The initial influence of the well is clear during the first seconds, tending to the aquifer slope at the end of the test, using a $\lambda = 0.008$ parameter with a Cauchy boundary condition. Obtained equivalent parameters with this interpretation are shown in Table 3.

Table 3. Results of analytical interpretation of the E1 test.

E1: Analytical method	K (m/s)	K (m ²)	K (Darcy)	Qc (m ³ /h)
Skin	2.53E-06	1.13E-13	0.17	5.5
Aquifer	1.67E-05	8.13E-13	1.13	

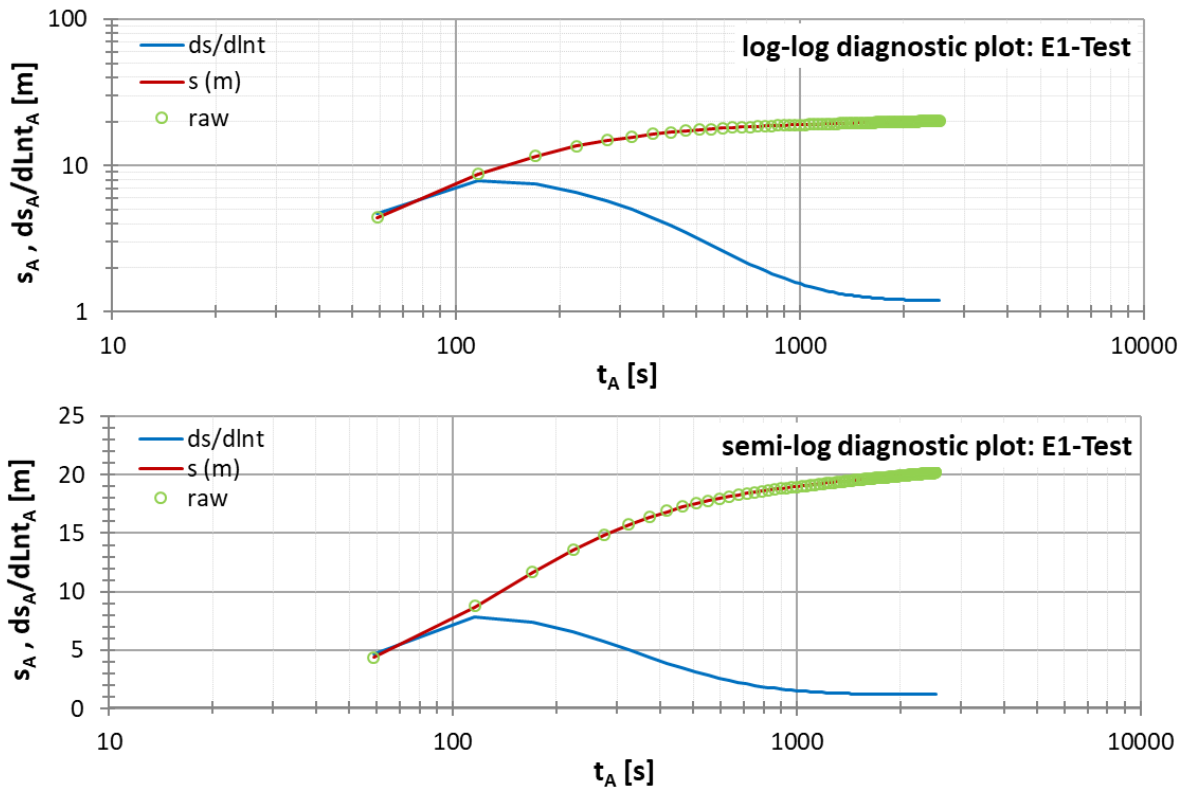


Figure 24. Sooth and filtered recovery data in semi-log and double-log graphics.

Table 4. E2 test main times.

E2-PT76	Data	Test time [d]	Test time [s]
Start time	9/9/2016 10:19	0	0
Stop pumping time	9/9/2016 15:26	0.21	18414
Final Recovery time	9/11/2016 1:33	1.63	141209

E2-PT78	Data	Test time [d]	Test time [s]
Start time	9/9/2016 10:19	0	0
Stop pumping time	9/9/2016 15:26	0.21	18414
Final Recovery time	9/11/2016 1:33	1.63	141209

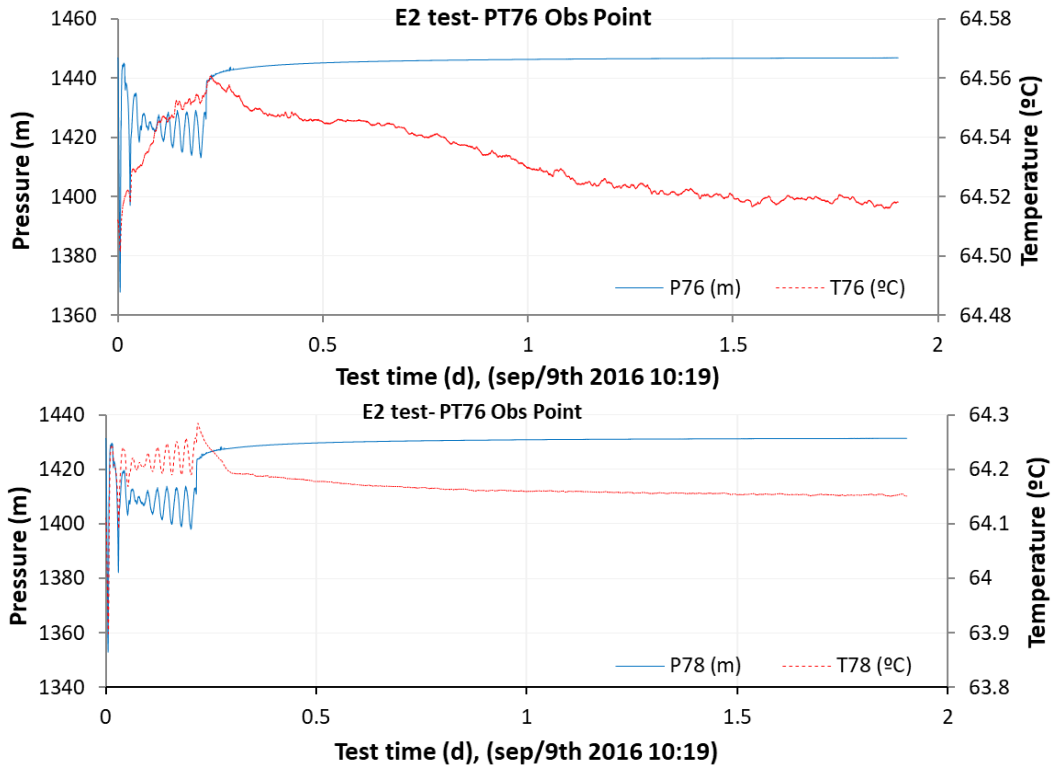


Figure 25. Pressure and temperature original E2 test data for 76 and 78 observation tests.

2.4.1.2 E2 test

For the interpretation of the E2 test, the measurements of the Pt76 and PT78 points are available (Figure 26). Mean test times are shown in Table 4, following pressure measurements.

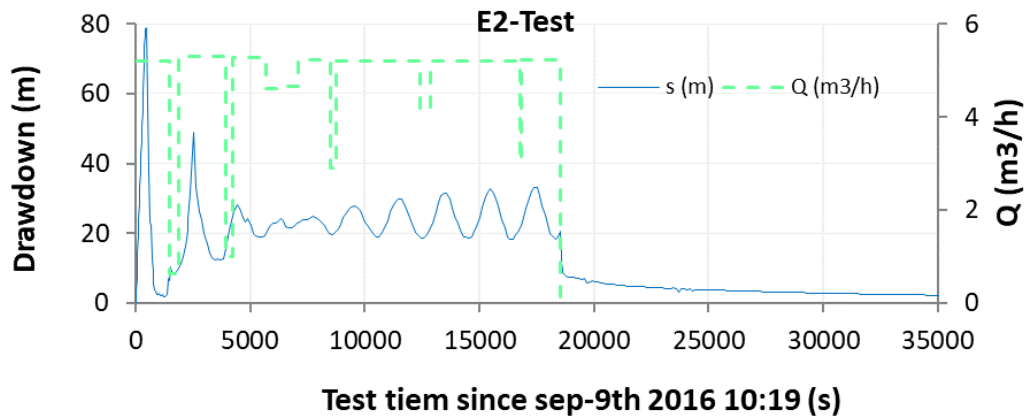


Figure 26. E2 flow rate steps (green dotted line) and drawdown (blue line).

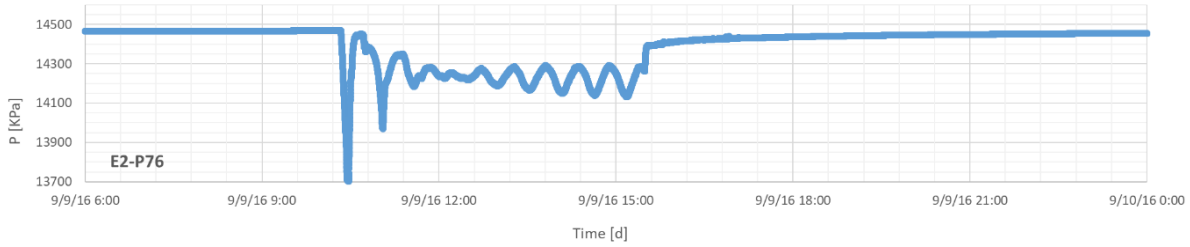


Figure 27. Comparison between pressure before and after hydraulic test.

On the other hand, pressure before and after the hydraulic test is constant, therefore no trend has been identified (Figure 27). Compute drawdowns for variable pumping rate using Trabucchi et al 2018 algorithm (Figure 28).

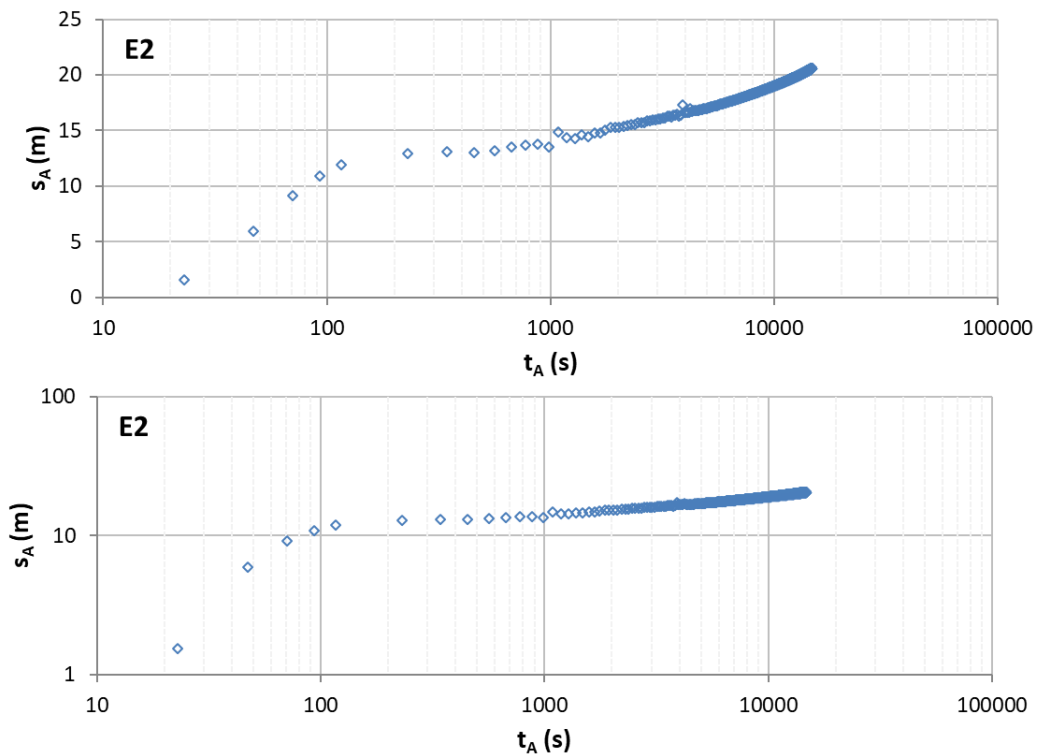


Figure 28. Drawdowns computed using Trabucchi method.

Table 5. Results of analytical interpretation of the E2 test.

E2: Analytical method	K (m/s)	K (m ²)	K (Darcy)	Qc (m ³ /h)
Skin	2.04E-06	9.95E-14	0.14	5.2
Aquifer	3.08E-06	1.50E-13	0.21	

On the step 3, the smoothing and filtering results are shown in Figure 29. Parameters used at this fit are: $\lambda=0.05$, with a Cauchy boundary condition, with a value of 0.14 at the outer boundary to reproduce the aquifer response. Obtained equivalent parameters with this interpretation are shown at Table 5.

2.4.1.3 E3 test

For the interpretation of the E3 test, the measurements of the Pt76 and PT78 points are available too (Figure 30), but only the later have been used because there are no sharp changes in pressure. Different flow-rate steps has been measured (Figure 31), establishing the correct times for test depending of the pressure answers (Table 6).

Table 6. E3 test main times.

E3-PT76	Data	Test time [d]	Test time [s]
Start time	29/09/2016 10:19	0	0
Stop pumping time	29/09/2016 15:26	0.22	18591
Final Recovery time	30/09/2016 1:33	1.51	130585

Trend correction has not been made, as in the E2 case, because no trends has been identified (Figure 32). Drawdowns has been calculated using Trabucchi et al (2108) method. Figure 33 represent this data on semi-log and log-log scale.

After smoothing and filtering original data first interpretation of test has been made (Figure 34). Parameters used at this fit are: $\lambda=0.002$ (Figure 35), with a Dirichlet boundary condition, with a value of 0.7 at the outer boundary to reproduce the aquifer response. Results are in Table 7.

Table 7. Results of analytical interpretation of the E3 test.

E3: Analytical method	K (m/s)	K (m ²)	K (Darcy)	Qc (m ³ /h)
Skin	1.17E-06	5.69E-14	0.08	7.2
Aquifer	2.18E-06	1.06E-13	0.15	8.2

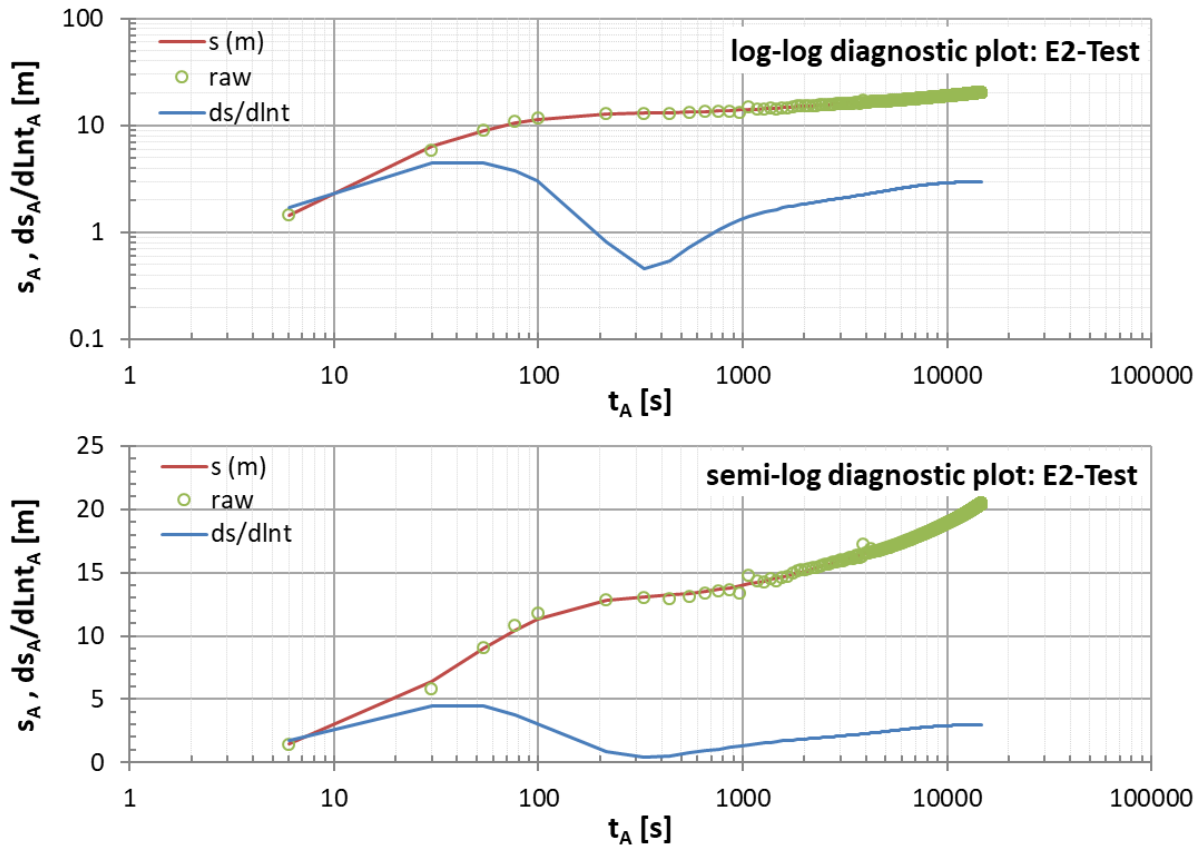


Figure 29. Agarwal interpretation recovery data in semi-log and double-log graphics.

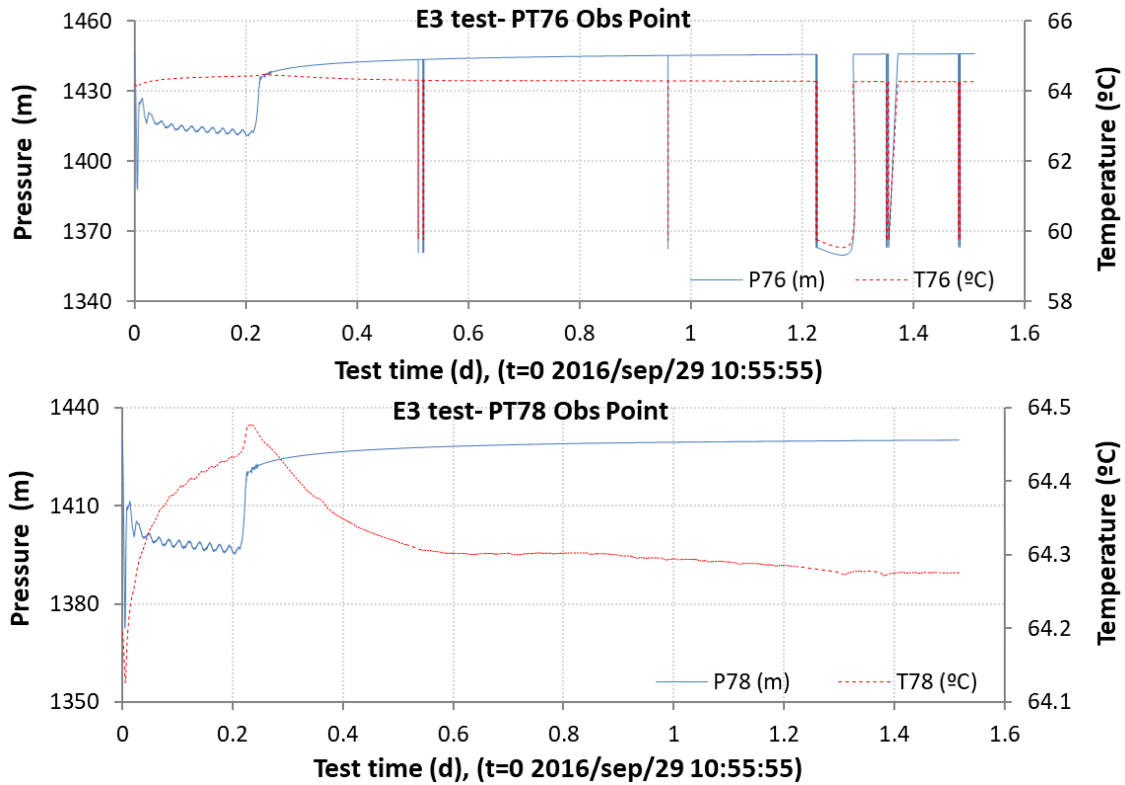


Figure 30. E3 pressure and temperature original data, for PT76 and PT 78 observation points.

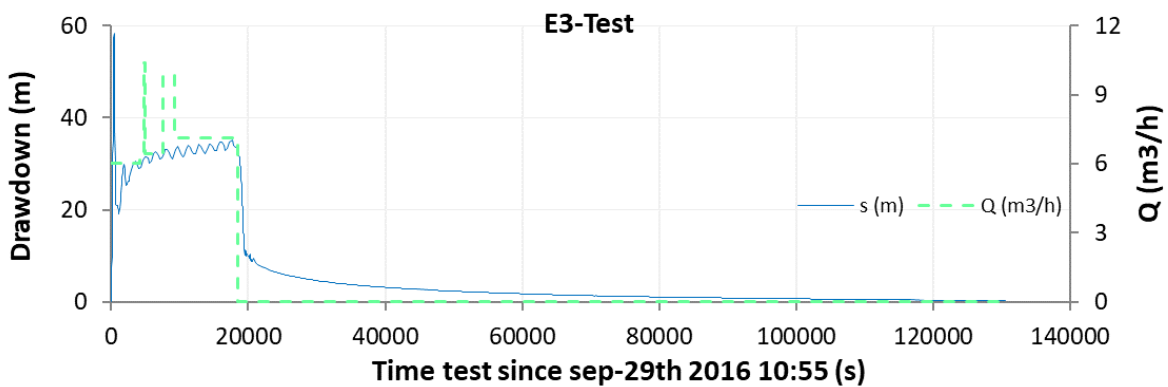


Figure 31. Flow rate steps and pressure measurement during test E3.

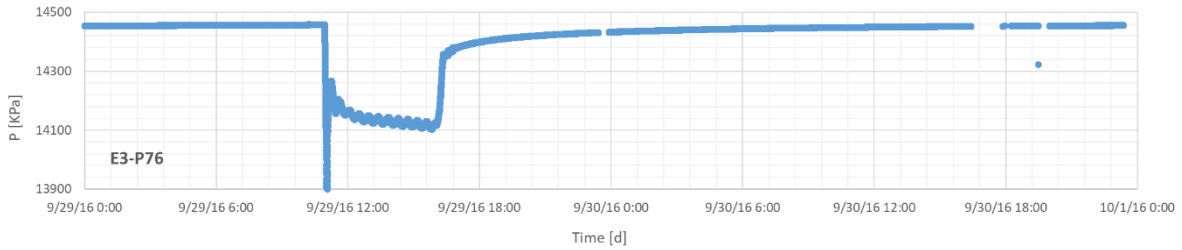


Figure 32. Comparison between pressure before and after hydraulic test.

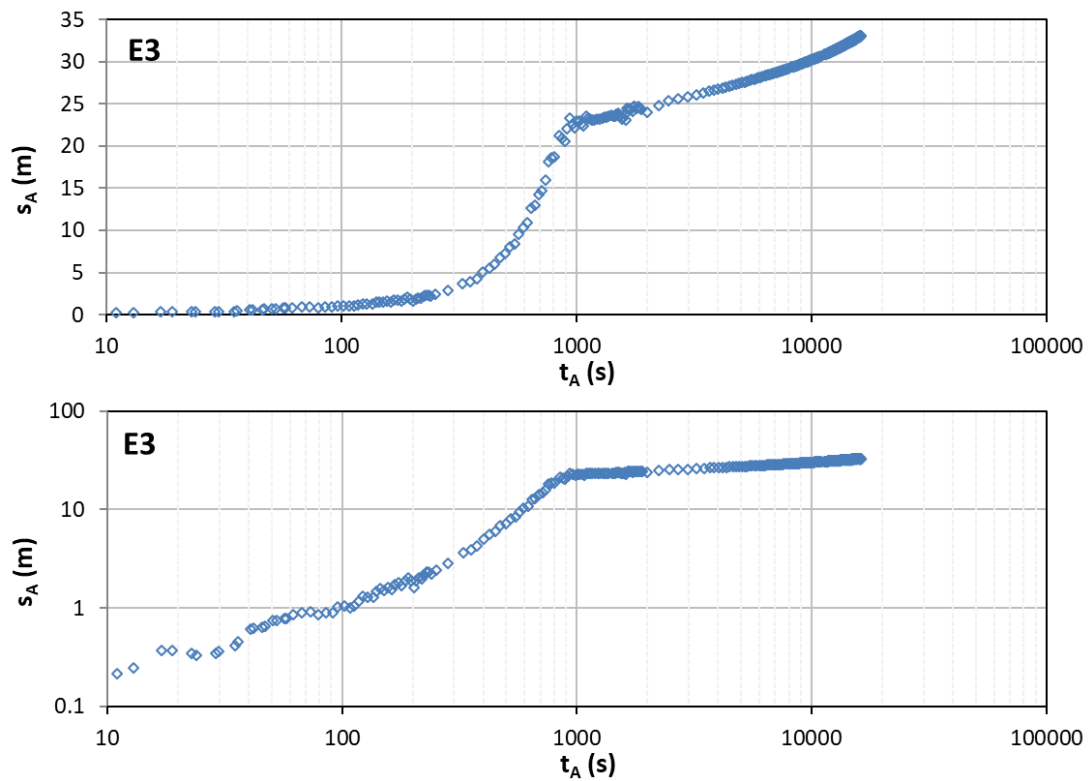


Figure 33. Drawdown calculated using Trabucchi method.

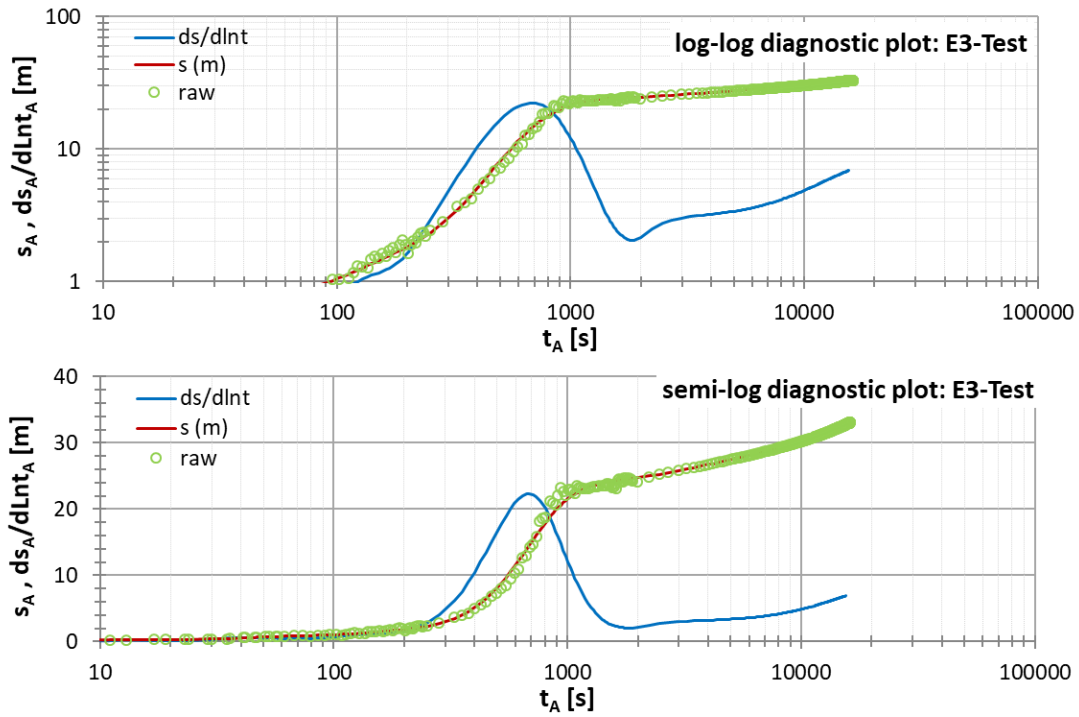


Figure 34. Agarwal interpretation of recovery data in semi-log and double-log graphics.

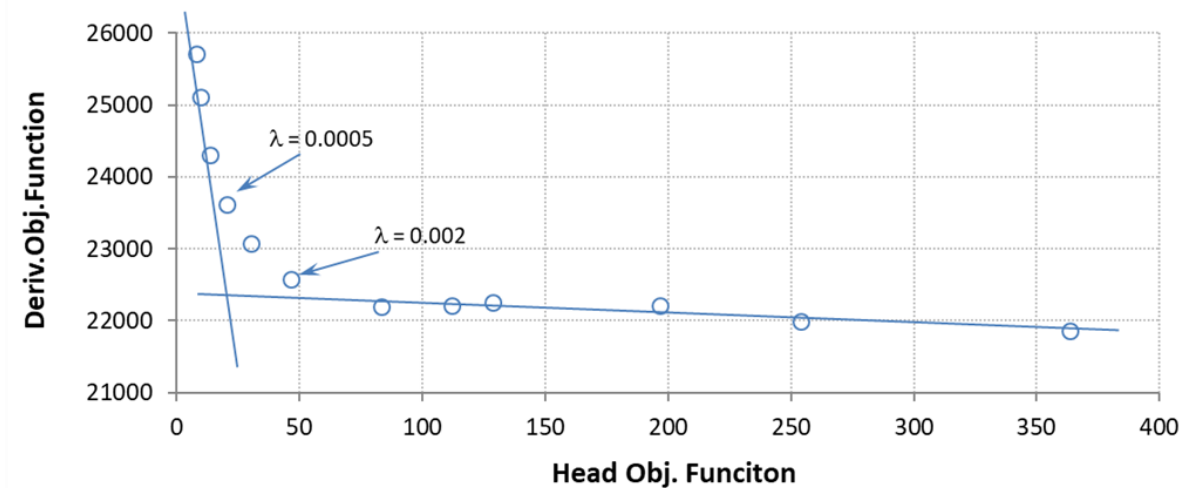


Figure 35. : Best value for $\lambda = 0.002$, for these measurements.

2.5 Numerical model

Tested interval has 14m thickness, isolating an aquifer formed by two layers of sand with a layer of clay between them, acting as an aquitard.

In order to obtain the hydraulic parameters, by zones (well, skin, CO₂ trapped zone and aquifer) it has been made a double 1D layer radial numerical model. This model consists of two 1D layers, representing the sand aquifers, connected by 1D elements acting as aquitard (clay). It reproduces the media using radial symmetry, with the well axis in the center. Boundary conditions are flowrate in the well wall, the outer boundary is located at 8km from the well, assuming no affection by the tests. No flow applies both at the upper and lower boundaries.

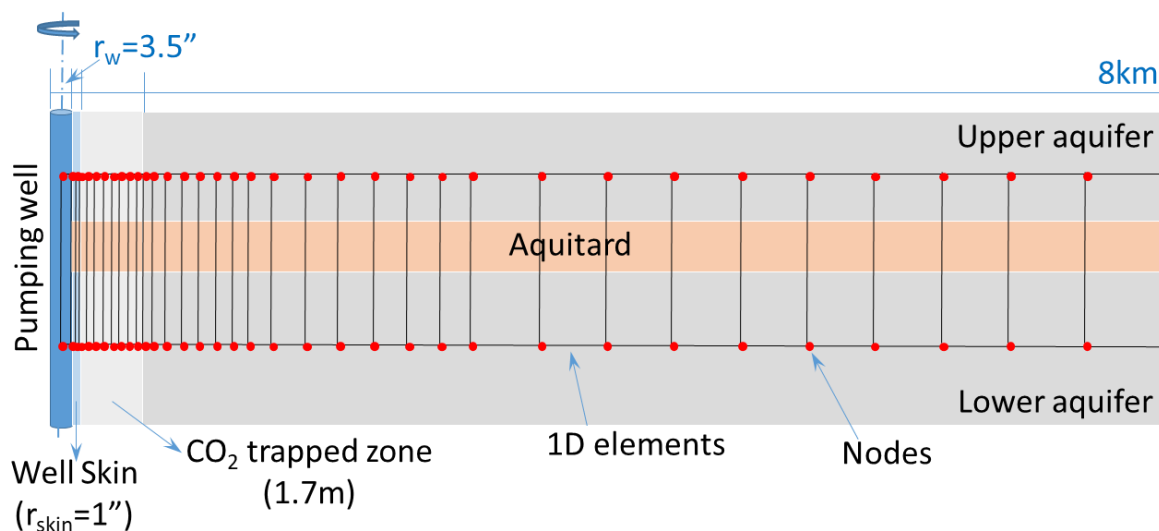


Figure 36. Synthetic geometry showing the main components of the model, so as a schematic mesh (nodes and elements).

The model represents the well (7" diameter), a thin skin (1" width), upper aquifer, lower aquifer, aquitard, and CO₂ trapped zone, this only in E3 test. The model was implemented in TRANSIN IV code (Medina and Carrera, 2003), a finite-element simulation and inversion code for groundwater flow and transport problems. The mesh contains 804 nodes and 1204 1D elements. Elements sizes increase from millimeters near the well to about 15m at the outer boundary.

The time discretization is the same for the 3 models, the observation and test parameters are the only difference between models.

The obtained results for each test are showed below.

2.5.1 E1 test

The response to this test draws the well effect, with a high permeability and storativity, at the first seconds.

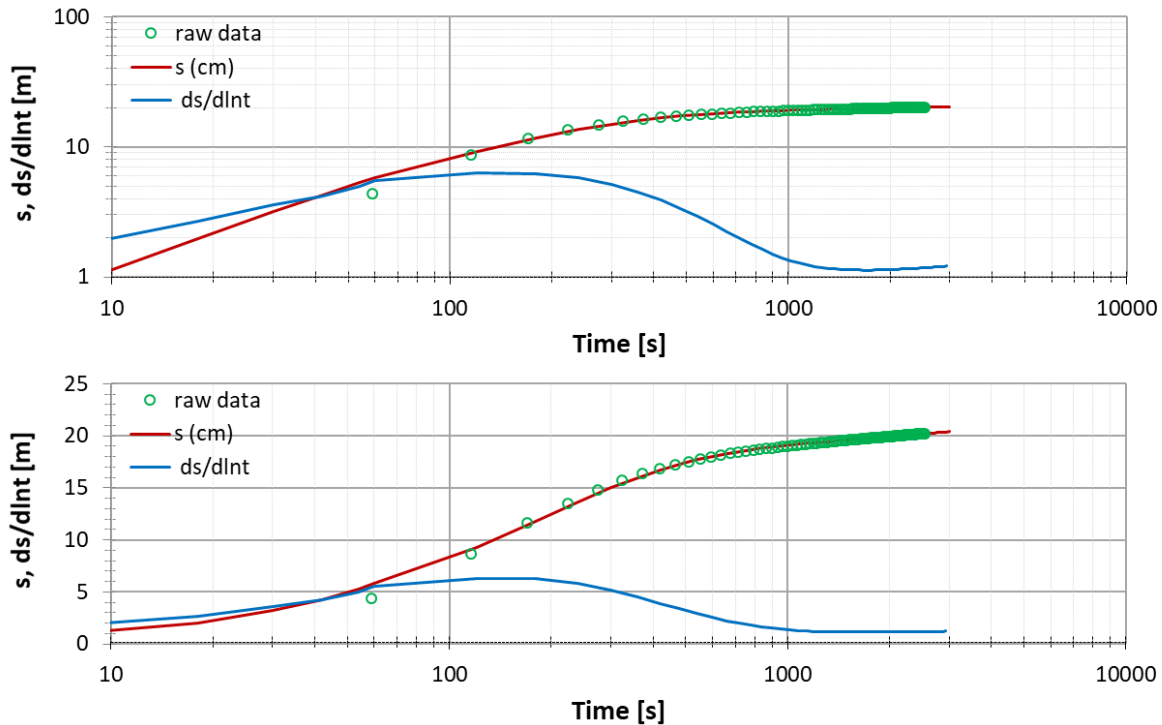


Figure 37. Numerical model E1 test interpretation. Raw data (green) refers to original data, and "s" to computed data. Both graphics represents the same data at double and semi-log scales.

Table 8. Comparison of result of analytical and numerical interpretation of the E1 test.

E1: Analytical method	K (m/s)	S (m ⁻¹)	K (m ²)	K (Darcy)
Skin		4.63E-2		
Aquifer	1.42E-07		6.89E-15	0.01
Up-Aquifer	3.01E-03	6.05E-07	1.46E-10	203.81
Aquitard	1.66E-10		8.08E-18	1.12E-05
Dw-Aquifer	3.18E-03		1.55E-10	215.45

Table 8 shows the parameter results for the two methods. Analytical method represent effective parameters, numerical method has a value for zone.

In the Figure 37 is clear the effect of the well, tending to the aquifer slope.

2.5.2 E2 test

At the second test the drawdowns display a curve very similar to those of E1, with a clear well effect at the beginning of the recovery, tending to the aquifer slope at the end. The model can fit very well these measurements (Figure 38 and Table 9).

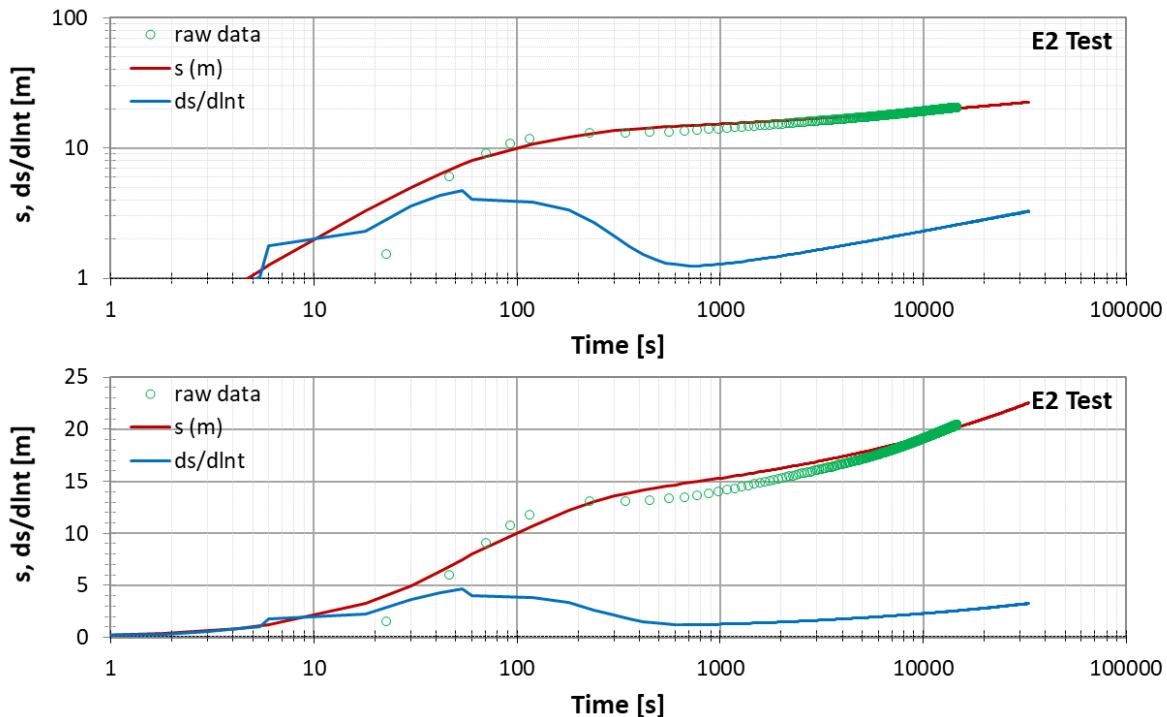


Figure 38. Numerical model E2 test interpretation. Raw data (green circles) refers to original data, and “s” to computed data. Both graphics represents the same data at double and semi-log scales.

Table 9. Comparison of result of analytical and numerical interpretation of the E2 test.

E2: Analytical method	K (m/s)	S (m ⁻¹)	K (m ²)	K (Darcy)
Skin		2.32E-2		
Aquifer	1.92E-07		9.36E-15	0.013
Up-Aquifer	7.67E-04	9.61E-06	3.73E-11	51.98
Aquitard	6.63E-07		3.23E-14	4.49E-02
Dw-Aquifer	2.83E-04		1.38E-11	19.20

2.5.3 E3 test

Calculated slopes from measured pressure draw two clear slopes (Figure 39). First slope refers to a variable flow-rate phase, at the beginning of the test. The second slope, draw a high derivative, that suggests a reduction of transmissivity in the region with CO₂, which is consistent with the relatively late time at which it occurs (high S, caused by the high compressibility of residual CO₂).

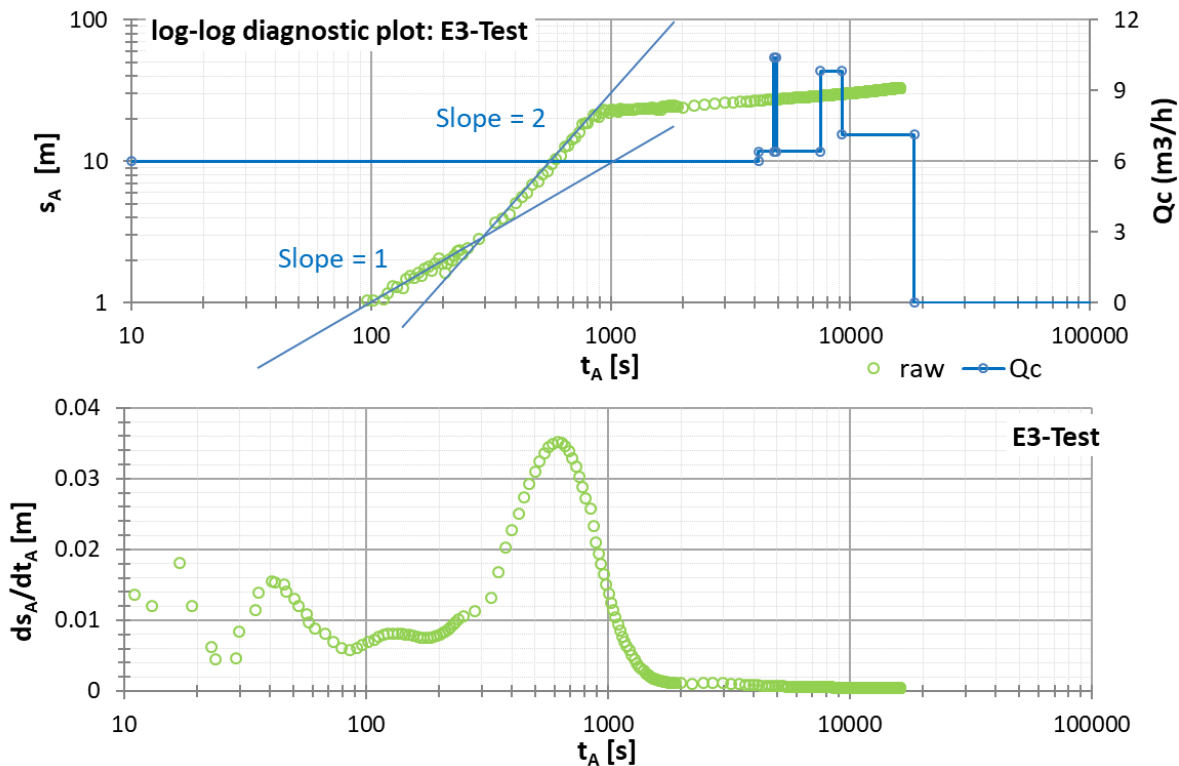


Figure 39. Measured data draw two different slopes (up), compared with its derivative (down).

Flow rate measurement have not been made with enough precision to reproduce these slopes (Figure 39), for this reason flow-rate has been reproduced using two time function at a time into the injection well, as show in Figure 40. Time t used is the time when the slope change.

The E3 test has been performed after a CO₂ push-pull test, which may explain why the results are different to the other tests (Figure 41 and Table 1).

The model fits the aquifer slope but it cannot do the same for the well zone. This may be because a CO₂ bubble has remained in the well.

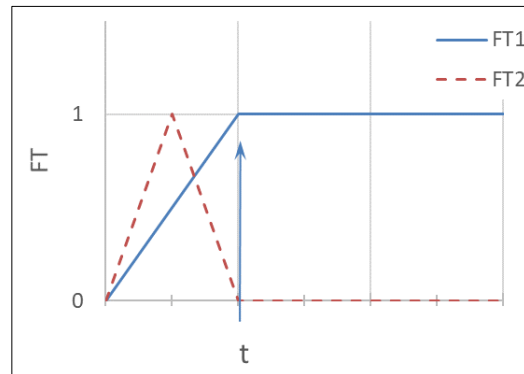


Figure 40. Time function used in flow-rate.

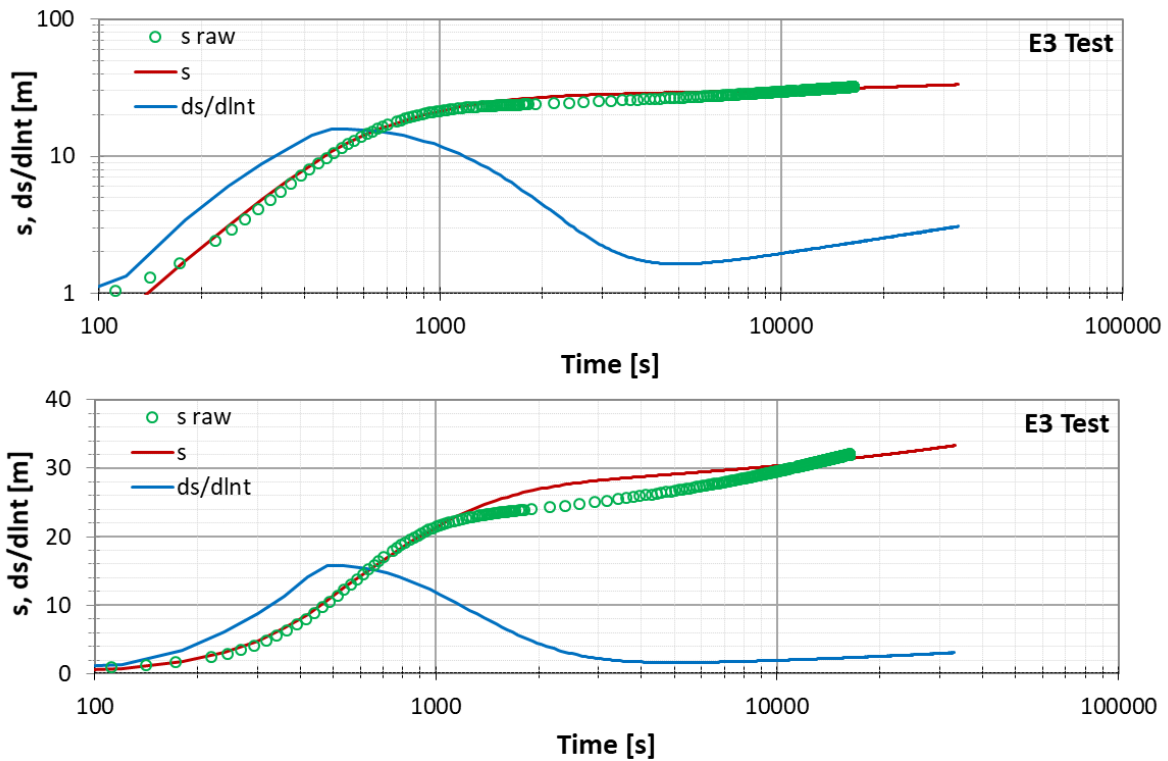


Figure 41. Numerical model E3 test interpretation. Raw data (green) refers to original data, and "com" to computed. Both graphics represents the same data at double and semi-log scales.

Table 10. Comparison of result of analytical and numerical interpretation of the E2 test.

E3: Analytical method	K (m/s)	S (m ⁻¹)	K (m ²)	K (Darcy)
Skin		9.25E-2		
Aquifer	1.44E-07	1.23E-07	7.01E-15	9.76E-03
Up-Aquifer	7.53E-04		3.67E-11	51.04
Aquitard	1.83E-10	4.28E-06	8.92E-18	1.24E-05
Dw-Aquifer	2.95E-04		1.44E-11	19.99
CO ₂ zone	8.91E-07	1.10E+00	4.37E-14	0.06

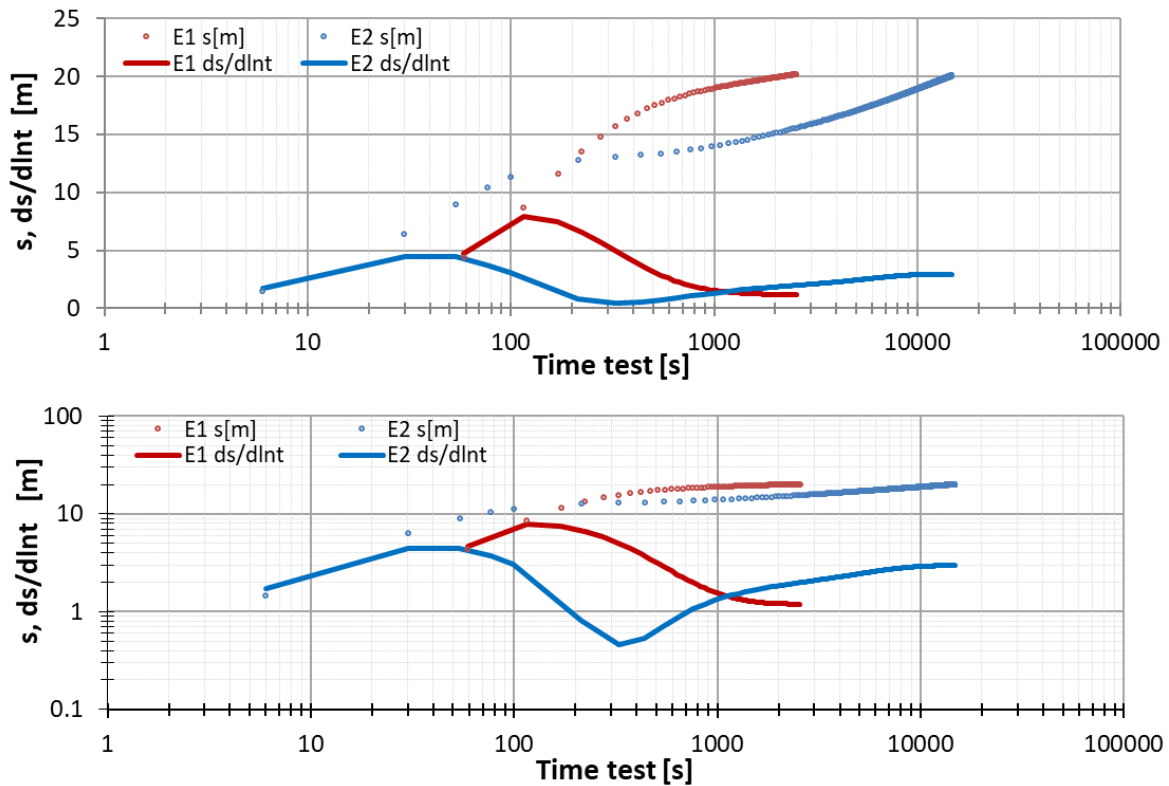


Figure 42. Comparison between E1 and E2 tests.

2.6 Discussion

This document compares the results obtained in three hydraulic tests. E1 and E2 tests were done before injecting CO₂ in the aquifer, whereas E3 was conducted after the CO₂ push pull test.

Comparing E1 and E2 tests (Figure 42 and Figure 44) the answer is very similar, with a slight difference close to the well (first seconds) that could be due to some changes in the aquifer just around the well.

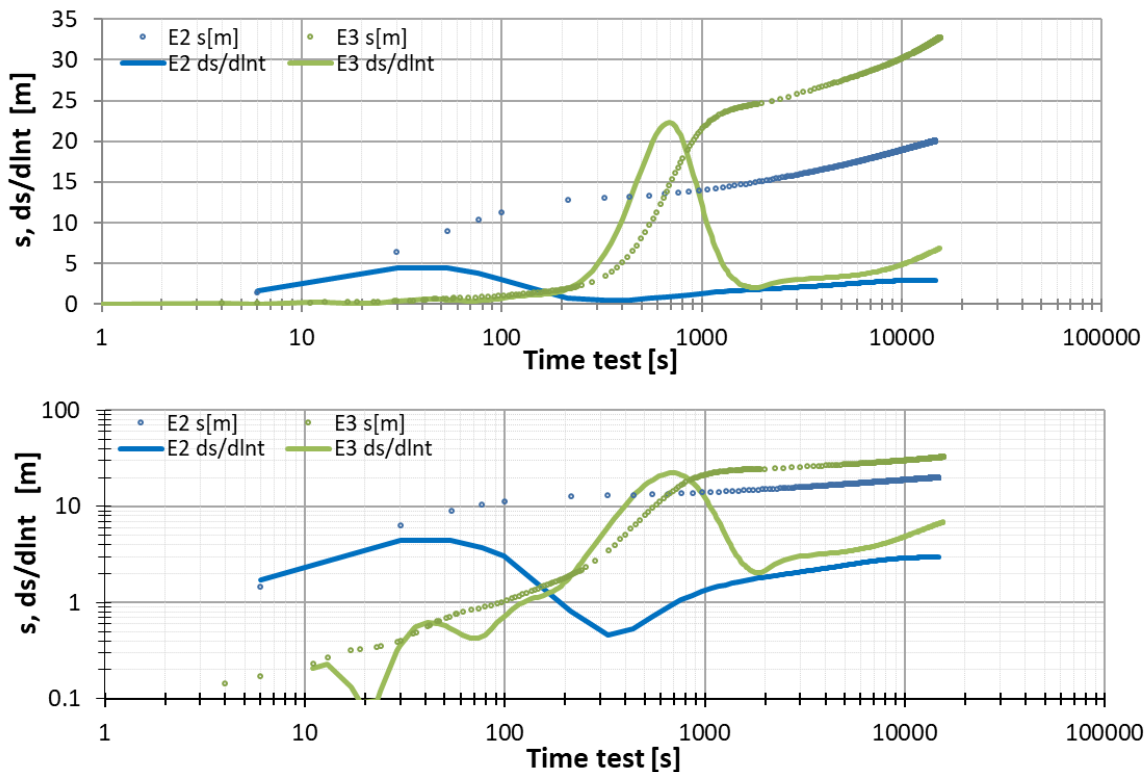


Figure 43. Hydraulic tests pressure measurements comparison. Recovery measurements data are represented by dots and his derivative by lines.

Tests E2 and E3 were performed with the aim of identifying the CO₂ trapping after one push-pull CO₂ test performed in the same interval. The shapes of the curves are quite different at the well, and all around it, but not in the aquifer, given that show the same slopes at the end in both responses (Figure 43 and Figure 44).

The first response in E3 test is delayed and exhibits a sharp increase of pressure. The storage coefficient (S) in the well is greater in E3, delaying the response, but the skin permeability has lower values in E3 than E2, causing this difference in pressures. This behavior can be explained by a small amount of residual CO₂ remaining around the well, generating a trapped bubble at the top of the interval.

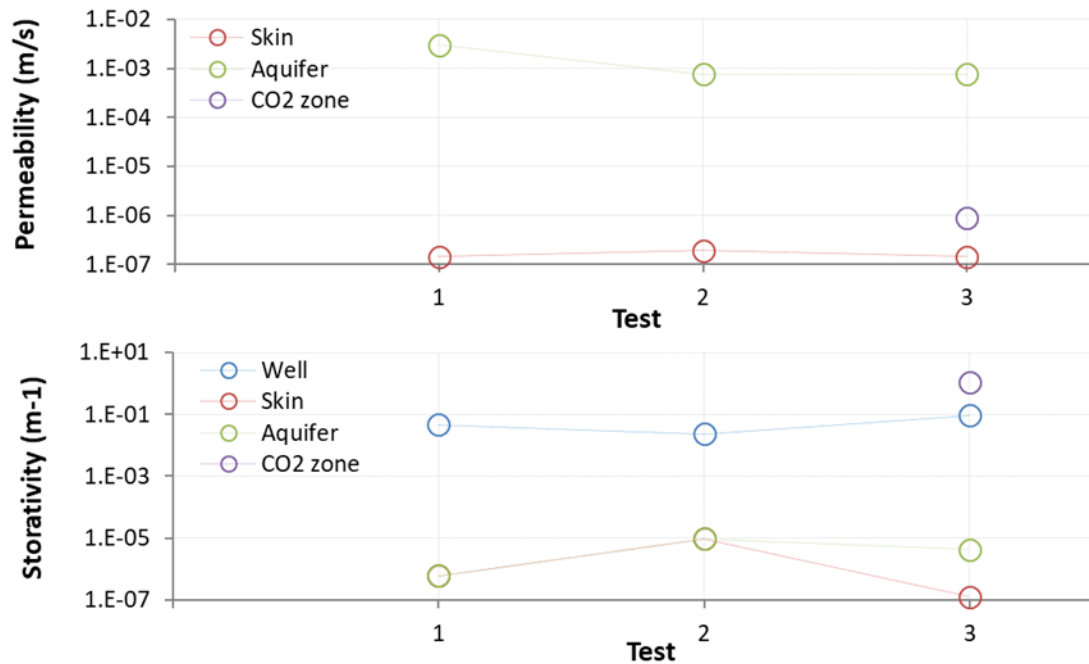


Figure 44. Tests E1, E2 and E3 calibration parameters comparisons are drawn, permeability values above and storativity below.

3. Conclusions

Two in-depth analyses have presented concerning specific details of Heletz Residual Trapping Experiment I (RTE I).

The first part (Chapter 1) presents a coupled wellbore-reservoir model for the period of CO₂ and CO₂/water self-release during the creation of the residually trapped zone. The observed behavior can be well matched by CO₂ exsolution in the well and reduced relative permeabilities in the formation, due to this exsolution. The model provides valuable supporting information concerning the overall behavior of the test and will later be incorporated with the overall reservoir model of RTE I (Deliverable 4.3).

The second part (Chapter 2) presents an in-depth analysis of the details of the hydraulic response of all the hydraulic tests carried out in the Heletz injection well, as part of the site characterization program and as part of RTE I. The results show that while the response of the two tests with no CO₂ in the system show a similar behaviour, the response from the test with residual CO₂ in the system is different. The storage coefficient in the well is greater, delaying the response, but the skin permeability has lower values. This behaviour can be explained by a small amount of residual CO₂ around the well, which is consistent with the other model analyses.

Both of these studies along with the studies presented in Deliverable 4.3 will together provide a good understanding of the residual trapping conditions at Heletz.

4. References: Section 1.

- Apps, J. A., L. Zheng, Y. Zhang, T. Xu & J. T. Birkholzer (2010) Evaluation of Potential Changes in Groundwater Quality in Response to CO₂ Leakage from Deep Geologic Storage. *Transport in Porous Media*, **82**, 215.
- da Silva, D. V. A. & J. D. Jansen (2015) A Review of Coupled Dynamic Well-Reservoir Simulation*1This research was carried out within the context of the ISAPP Knowledge Centre. ISAPP (Integrated Systems Approach to Petroleum Production) is a joint project of TNO, Delft University of Technology, ENI, Statoil and Petrobras. *IFAC-PapersOnLine*, **48**, 236.
- Hingerl, F. F., F. Yang, R. Pini, X. Xiao, M. F. Toney, Y. Liu & S. M. Benson (2016) Characterization of heterogeneity in the Heletz sandstone from core to pore scale and quantification of its impact on multi-phase flow. *International Journal of Greenhouse Gas Control*, **48, Part 1**, 69.
- Hu, B. (2007) Integrated Wellbore-Reservoir Dynamic Simulation. *Asia Pacific Oil and Gas Conference and Exhibition*.
- IPCC, (2005) IPCC Special Report on carbon dioxide capture and storage. Cambridge.
- Lu, X., A. Watson, A. V. Gorin & J. Deans (2005) Measurements in a low temperature CO₂-driven geysiring well, viewed in relation to natural geysers. *Geothermics*, **34**, 389.
- Lu, X., A. Watson, A. V. Gorin & J. Deans (2006) Experimental investigation and numerical modelling of transient two-phase flow in a geysiring geothermal well. *Geothermics*, **35**, 409.
- Niemi, A., J. Bensabat, V. Shtivelman, K. Edlmann, P. Gouze, L. Luquot, F. Hingerl, S. M. Benson, P. A. Pezard, K. Rasmusson, T. Liang, F. Fagerlund, M. Gendler, I. Goldberg, A. Tatomir, T. Lange, M. Sauter & B. Freifeld (2016) Heletz experimental site overview, characterization and data analysis for CO₂ injection and geological storage. *International Journal of Greenhouse Gas Control*, **48**, 3.
- Pan, L. & C. M. Oldenburg (2014) T2Well-An integrated wellbore-reservoir simulator. *Computers and Geosciences*, **65**, 46.
- Pan, L., C. M. Oldenburg, K. Pruess & Y.-S. Wu (2011a) Transient CO₂ leakage and injection in wellbore-reservoir systems for geologic carbon sequestration. *Greenhouse Gases: Science and Technology*, **1**, 335.
- Pan, L., C. M. Oldenburg, Y.-S. Wu & K. Pruess, (2011b) T2Well/ECO₂N Version 1.0: Multiphase and Non-isothermal Model for Coupled Wellbore-reservoir Flow of Carbon Dioxide and Variable Salinity Water. LBNL-4291E (Ed.).

- Pan, L., S. W. Webb & C. M. Oldenburg (2011) Analytical solution for two-phase flow in a wellbore using the drift-flux model. *Advances in Water Resources*, **34**, 1656.
- Rasmusson, K., M. Rasmusson, F. Fagerlund, J. Bensabat, Y. Tsang & A. Niemi (2014) Analysis of alternative push-pull-test-designs for determining in situ residual trapping of carbon dioxide. *International Journal of Greenhouse Gas Control*, **27**, 155.
- Rasmusson, K., C.-F. Tsang, Y. Tsang, M. Rasmusson, L. Pan, F. Fagerlund, J. Bensabat & A. Niemi (2015) Distribution of injected CO₂ in a stratified saline reservoir accounting for coupled wellbore-reservoir flow. *Greenhouse Gases: Science and Technology*, **5**, 419.
- Shi, H., J. A. Holmes, L. J. Durlofsky, K. Aziz, L. Diaz, B. Alkaya & G. Oddie (2005) Drift-Flux Modeling of Two-Phase Flow in Wellbores.
- Watson, Z. T., W. S. Han, E. H. Keating, N.-H. Jung & M. Lu (2014) Eruption dynamics of CO₂-driven cold-water geysers: Crystal, Tenmile geysers in Utah and Chimayó geyser in New Mexico. *Earth and Planetary Science Letters*, **408**, 272.
- Xu, R., R. Li, F. Huang & P. Jiang (2017) Pore-scale visualization on a depressurization-induced CO₂ exsolution. *Science Bulletin*, **62**, 795.
- Zuo, L., J. B. Ajo-Franklin, M. Voltolini, J. T. Geller & S. M. Benson (2017) Pore-scale multiphase flow modeling and imaging of CO₂ exsolution in Sandstone. *Journal of Petroleum Science and Engineering*, **155**, 63.
- Zuo, L., S. Krevor, R. W. Falta & S. M. Benson (2012) An Experimental Study of CO₂ Exsolution and Relative Permeability Measurements During CO₂ Saturated Water Depressurization. *Transport in Porous Media*, **91**, 459.
- Zuo, L., C. Zhang, R. W. Falta & S. M. Benson (2013) Micromodel investigations of CO₂ exsolution from carbonated water in sedimentary rocks. *Advances in Water Resources*, **53**, 188.

Section 2.

- Agarwal, R.G. (1980). A New Method To Account For Producing Time Effects When Drawdown Type Curves Are Used To Analyze Pressure Buildup And Other Test Data. SPE Annual Technical Conference and Exhibition, p.20 pp. doi: 10.2118/9289-MS.
- Andersen, R.S. and Hoog, F.R. (1984), Finite difference methods for the numerical differentiation of non-exact data. *Computing*, 33(3-4), 259-267.
- Ashjari, J. (2013). Determination of storage coefficients during pumping and recovery. *Groundwater*, 51(1), pp.122–127. doi: 10.1111/j.1745-6584.2012.00917.x.
- Ballukraya, P.N. & Sharma, K.K. (1991). Estimation of storativity from recovery data. *Groundwater*, 29(4), pp.495–498. doi: 10.1111/j.1745-6584.1991.tb00540.x.

- Banton, O. & Bangoy, L.M. (1996). A new method to determine storage coefficient from pumping test recovery data. *Groundwater*, 34(5), pp.772–777. doi:10.1111/j.1745-6584.1996.tb02069.x.
- Beauheim, R. L.(1988), Scale effects in well testing in fractured media, 4. annual Canadian/American conference on hydrogeology, Banff, Canada, 22 Jun 1988.
- Beauheim, R. L., Roberts, R. M., and Avis J. D, (2004), Well testing in fractured media: flow dimensions and diagnostic plots, *J. Hyd. Res.*, 42, 69-76.
- Bernard, S., Delay, F., and Porel, G. (2006), A new method of data inversion for the identification of fractal characteristics and homogenization scale from hydraulic pump test in fractured aquifers, *Journal of Hydrology*, 328, 647-658.
- Birsoy, Y.K. & Summers, W.K. (1980). Determination of aquifer parameters from step tests and intermittent pumping data. *Groundwater*, 18(2), pp.137–146. doi: 10.1111/j.1745-6584.1980.tb03382.x.
- Bourdet, D. et al. (1983). A new set of type curves simplifies well test analysis. *World oil*, 196(6), pp.95–106. doi: 10.2118/12777-PA.
- Bourdet, D., Ayoub, J.A. & Pirard, Y.M. (1989). Use of Pressure Derivative in Well Test Interpretation. *SPE Formation Evaluation*, 4(2), pp.293–302. doi: 10.2118/12777-PA.
- Butler J. J., Healey J. M. (1988), Relationship between pumping-test and slug-test parameters: scale effect or artifact? 63(2), *Ground Water*, 305-312.
- Camacho-Velazquez, R. , M. Vásquez-Cruz, R. Castrejón-Aviar, V. Arana-Ortiz (2005), Pressure transient and decline curve behavior in naturally vuggy carbonate reservoirs, *SPE Reservoir Evaluation & Engineering*, Vol. 8, N. 2, April 2005.
- Cao, M., Xu, W., Ostachowicz, W., & Su, Z. (2014). Damage identification for beams in noisy conditions based on Teager energy operator-wavelet transform modal curvature. *J. Sound and Vibration*, 333(6), 1543-1553.
- Carrera, J., and S. P. Neuman (1986), Estimation of Aquifer Parameters Under Transient and Steady State Conditions: 1. Maximum Likelihood Method Incorporating Prior Information, *Water Resour. Res.*, 22(2), 199–210, doi:10.1029/WR022i002p00199
- Castellanos J.L, Gomez, S. and Guerra, V., (2002), The triangle method for finding the corner of the L-curve, *Applied Numerical Mathematics*, 43, 359-373.
- Chang, J. and Y.C. Yortsos (1990), Pressure transient analysis of fractal reservoirs. *SPE Formation Evaluation*, 5(01), 31-38.
- Chartrand R. (2011), Numerical differentiation of noisy, nonsmooth data, *ISRN Applied Mathematics*, Article ID 165564.
- Chenaf, D. & Chapuis, R.P. (2002). Methods to determine storativity of infinite confined aquifers from a recovery test. *Groundwater*, 40(4), pp.385–389. doi: 10.1111/j.1745-6584.2004.tb02459.x.

- Chow, V. T. (1952), On the determination of transmissibility and storage coefficients from pumping test data. *Eos, Trans. Am. Geoph. Union*, 33(3), 397-404.
- Çimen, M. (2015). A straight-line method for analyzing residual drawdowns at an observation well. *Mathematical Problems in Engineering*, 2015(1), pp.1–6. doi:10.1155/2015/978040.
- Cooper, H.H. & Jacob, C.E. (1946). A generalized graphical method for evaluating formation constants and summarizing well- field history. *Eos, Transactions American Geophysical Union*, 27(4), pp.526–534. doi: 10.1029/TR027i004p00526.
- Coppola Jr, E., Szidarovszky, F., Poulton, M., Emery C. (2003). Artificial neural network approach for predicting transient water levels in a multilayered groundwater system under variable state, pumping, and climate conditions. *Journal of Hydrologic Engineering*, 8(6), 348-360.
- Coppola, E. A., Rana, A. J., Poulton, M. M., Szidarovszky, F., Uhl, V. W. (2005). A neural network model for predicting aquifer water level elevations. *Groundwater*, 43(2), 231-241.
- Copt, N.K. et al. (2011). Inferring spatial distribution of the radially integrated transmissivity from pumping tests in heterogeneous confined aquifers. *Water Resources Research*, 47(5), pp.1–11. doi: 10.1029/2010WR009877.
- Cullum, J. (1971) Numerical differentiation and regularization, *SIAM J. Numer. Anal.*, 8(2).
- Earlougher, R.C. & Kersch, K.M. (1974). Analysis of Short-Time Transient Test Data By Type-Curve Matching. *Journal of Petroleum Technology*, 26(7), pp.739-800. doi: 10.2118/4488-PA.
- Freeze, R. A., Cherry, J. A. (1979). *Groundwater*. Prentice—Hall, Inc. Englewood cliffs, New Jersey.
- Gomez, S., Ramos, G., Mesejo, J. A., Camacho, R., Vazquez, M. and Del Castillo, N. (2014) Well Test Analysis of Naturally Fractured Vuggy Reservoirs with an Analytical Triple Porosity-Double Permeability Model and a Global Optimization Method, *Oil & Gas Science and Technology* 69(4):653-671.
- Gringarten, A. C., Ramey Jr, H. J., and Raghavan, R. (1974). Unsteady-state pressure distributions created by a well with a single infinite-conductivity vertical fracture. *Soc. Petrol. Eng. J.*, 14(4), 347-360.
- Gringarten, A.C. et al. (1979). A comparison between different skin and wellbore storage type-curves for early-time transient analysis. In *SPE Annual Technical Conference and Exhibition*. Society of Petroleum Engineers. doi:10.2118/8205-MS.
- Gringarten, A.C. (2008). From straight lines to deconvolution: The evolution of the state of the art in well test analysis. *SPE Reservoir Evaluation & Engineering*, 11(1), pp.41–62. doi:10.2118/102079-PA.
- Halford, K. et al. (2012). Advanced methods for modeling water-levels and estimating drawdowns with SeriesSEE, an Excel add-In, (ver. 1.1, July, 2016): U.S. Geological Survey Techniques and Methods 4–F4, 28 p. <https://dx.doi.org/10.3133/tm4F4>.

- Halford, K.J., Weight, W.D. & Schreiber, R.P. (2006). Interpretation of Transmissivity Estimates from Single-Well Pumping Aquifer Tests. *Ground Water*, 44(3), pp.467–471. doi: 10.1111/j.1745-6584.2005.00151.x.
- Hosseinpour-Zonoozi, N., Ilk, D., Blasingame, T. A. (2006), The Pressure Derivative Revisited-- Improved Formulations and Applications. *Soc. Petrol. Eng. SPE paper 103204*.
- Indelman, P., & Dagan, G. (1993). Upscaling of permeability of anisotropic heterogeneous formations: 1. The general framework. *Wat. Resour. Res.*, 29(4), 917-923.
- Kitanidis, P. K. (2007) On Stochastic Inverse Modeling, in *Subsurface Hydrology: Data Integration for Properties and Processes* (eds D. W. Hyndman, F. D. Day-Lewis and K. Singha), American Geophysical Union, Washington, D. C.. doi: 10.1029/171GM04.
- Knowles I. and R. Wallace (1995) A variational method for numerical differentiation, *Numerische Mathematik* 70:91-110,.
- Knowles I. and R. J. Renka (2014), Methods for numerical differentiation of noisy data, *Electronic Journal of Differential Equations*, Conference 21, 235-246
- Kruseman, G.P. & de Ridder, N.A. (1990). *Analysis and Evaluation of Pumping Test Data*. 2nd ed., International Institute for Land Reclamation and Improvement.
- Luccarini, L., Bragadin, G. L., Colombini, G., Mancini, M., Mello, P., Montali, M., & Sottara, D. (2010). Formal verification of wastewater treatment processes using events detected from continuous signals by means of artificial neural networks. Case study: SBR plant. *Environmental Modelling & Software*, 25(5), 648-660.
- Machado, J. T. (2009). Calculation of fractional derivatives of noisy data with genetic algorithms. *Nonlinear Dynamics*, 57(1-2), 253-260.
- Martinez-Landa, L., Rötting, T.S., Carrera, J., Russian, A., Dentz, M., and Cubillo, B. 2013. Use of hydraulic tests to identify the residual CO₂ saturation at a geological storage site. *International Journal of Greenhouse Gas Control*. <http://dx.doi.org/10.1016/j.ijggc.2013.01.043>.
- Meier, P.M. et al. (1998). An evaluation of Jacob's method for the interpretation of pumping tests in heterogeneous formations. *Water Resources Research*, 34(5), pp.1011–1025. doi: 10.1029/98WR00008.
- Mishra, P.K., Vessilinov, V. & Gupta, H. (2013). On Simulation and Analysis of Variable- Rate Pumping Tests. *Groundwater*, 51(3), pp.469–473. doi: 10.1111/j.1745-6584.2012.00961.x
- Neuman, S. P., Witherspoon, P. A. (1970). Variational principles for confined and unconfined flow of ground water. *Wat. Resour. Res.*, 6(5), 1376-1382.
- Neuman, S. P., Witherspoon, P. A. (1972). Field determination of the hydraulic properties of leaky multiple aquifer systems. *Wat. Resour. Res.*, 8(5), 1284-1298.
- Neuman, S. P., & De Marsily, G. (1976). Identification of linear systems response by parametric programming. *Wat. Resour. Res.*, 12(2), 253-262.

- Niemi, A., Bensabet, J., Shtivelman, V., Edlmann, K., Gouze, P., Luquot, L., Hingerl, F., Benson, S.M., Pezard, P.A., Rasmusson, K., Liang, T., Fagerlund, F., Gendler, M., Goldberg, I., Tatomir, A., Lange, T., Saute, M., Freifeld, B. (2016). Heletz experimental site overview, characterization and data analysis for CO₂ injection and geological storage. *Int.J.Greenhouse Gas Control*, <http://dx.doi.org/j.ijggc.2015.12.030>.
- Rai, S. P. (1985), Numerical determination of aquifer constants. *Journal of Hydraulic Engineering ASCE*, 111(7), 1110-1114.
- Ramey, H.J. (1970). Short-time well test data interpretation in the presence of skin effect and wellbore storage. *Journal of Petroleum Technology*, 22(1), pp.97–104. doi:10.2118/2336-PA.
- Ramos, G., Carrera, J., Gómez, S., Minutti, C., and Camacho, R. 2017. A stable computation of log-derivatives from noisy drawdown data. *Water Resources Research*. <http://dx.doi.org/10.1002/2017WR020811>.
- Renard, P. (2005). The future of hydraulic tests. *Hydrogeol. J.*, 13(1), 259-262.
- Renard, P., Glenz, D. & Mejias, M. (2009). Understanding diagnostic plots for well-test interpretation. *Hydrogeology Journal*, 17(3), pp.589–600. doi: 10.1007/s10040-008-0392-0.
- Schroeter, T. Von et al. (2002). Analysis of well test data from permanent downhole gauges by deconvolution. In *SPE Annual Technical Conference and Exhibition*. Society of Petroleum Engineers. doi:10.2118/77688-MS.
- Sen, Z. (1986), Determination of Aquifer Parameters by the Slope- Matching Method. *Ground Water*, 24(2), 217-223.
- Sun, X., Xu, Y., Lin, L. (2015). The diagnostic plot analysis of artesian aquifers with case studies in Table Mountain Group of South Africa. *Hydrogeol. J.*, 23(3), 567-579.
- Srivastava, R. and A. Guzman- Guzman (1998), Practical approximations of the well function. *Ground Water*, 36(5), 844-848.
- Theis, C. V (1935). The relation between the lowering of the Piezometric surface and the rate and duration of discharge of a well using ground- water storage. *Eos, Transactions American Geophysical Union*, 16(2), pp.519–524. doi: 10.1029/TR016i002p00519.
- Trabucchi, M. and Carrera, J. 2018. Generalizing Agarwal’s method for the interpretation of recovery tests under non-ideal conditions...
- Willmann, M. et al. (2007). On the meaning of the transmissivity values obtained from recovery tests. *Hydrogeology Journal*, 15(5), pp.833–842. doi: 10.1007/s10040-006-0147-8.
- Xiao, L., & Xu, Y. (2014). Diagnostic Analysis of Pumping Tests Using Derivative of dlgs/dlgt with Case Study. *Groundwater*, 52(S1), 208-217.
- Yeh, H. D. (1987). Theis' Solution by Nonlinear Least- Squares and Finite- Difference Newton's Method. *Ground Water*, 25(6), 710-715.



Zheng, L., Guo, J.J. & Lei, Y. (2005). An Improved Straight- Line Fitting Method for Analyzing Pumping Test Recovery Data. *Groundwater*, 43(6), pp.939–942. doi: 10.1111/j.1745-6584.2005.00094.x.